C.P. No. 816

MINISTRY OF AVIATION

AERONAUTICAL RESEARCH COUNCIL

CURRENT PAPERS

Measurements of Dynamic Stability from Three Simplified Free-Flight Models of a Supersonic Research Aircraft (Bristol T. 188) over the Mach Number Range 1.2 - 2.6

by

K. J. Turner

LONDON: HER MAJESTY'S STATIONERY OFFICE

1965

PRICE 10s 6d NET

U.D.C. No. 533.6.013.412 : 533.6.013.413 : 533.6.011.5 :
533.6.055 : 533.652.1

C.P. No.816

March, 1961

MEASUREMENTS OF DYNAMIC STABILITY FROM THREE SIMPLIFIED FREE-FLIGHT MODELS OF A SUPERSONIC RESEARCH AIRCRAFT (BRISTOL T.188) OVER THE MACH NUMBER RANGE 1.2 - 2.6

by

K. J. Turner

SUMMARY

Values of the lateral stability derivatives y_v, n_v, ℓ_v and ℓ_p have been measured on free-flight models of the Bristol T.188 for Mach numbers between 1.2 and 2.6. These show that the aircraft should be laterally stable up to M = 2.6, at least, although the free-flight results indicate a somewhat smaller stability margin than estimates or wind-tunnel measurements.

Some additional data on z_w and m_w have been derived from the longitudinal motion.

Replaces R.A.E. Report No. Aero. 2648 - A.R.C. 23 295.

LIST OF CONTENTS

		Page
1	INTRODUCTION	5
2	DESCRIPTION OF THE MODELS	5
3	FLIGHT BEHAVIOUR	7
4	METHODS OF ANALYSIS	8
	4.1 Basic principles	8
	4.2 Lateral stability	9
	4.2.1 Analytic solution (method A)	9
	4.2.2 Vector solution (method B)	10
	4.2.3 Simplified solutions (methods C,D,E)	11
	4.2.4 Direct solution for y_v (method F)	12
	4.3 Longitudinal stability	12
	4.4 Corrections for centre of gravity shift	13
5	DISCUSSION OF RESULTS	13
	5.1 Lateral stability	13
	5.2 Longitudinal stability	16
6	CONCLUSIONS	17
LIST OF SYMBOLS		18-20
LIST OF REFERENCES		21
TABLES 1 AND 2		22-23
ILLUSTRATIONS - Figs.1-42		-
DETACHABLE ABSTRACT CARDS		-

LIST OF TABLES

Table		
1	- Model data	22
2	- Model instrumentation	23

LIST OF ILLUSTRATIONS

	Fig.
The full-scale aircraft	1
General arrangement of models 1 and 2	2
General arrangement of model 3	3
Photographs of models	4(a-e)

LIST OF ILLUSTRATIONS (Contd)

	Fig.
Body profiles	5
Wing details	6
Fin details	7(a,b)
Nacelle details	8(a,b)
Trajectories (models 1,2,3)	9
Velocity (models 1,2,3)	10
Mach number (models 1,2,3)	11
Range of Reynold's number (models 1,2,3)	12
Superimposed steady rate of roll	13
Mean side-force coefficient	14
Mean sideslip angle	15
Mean lift coefficient (models 1,2,3)	16
Mean incidence (model 3)	17
Sample of telemetry record	18
Sample of data for determining frequency and phase relationships of the Dutch-roll oscillation (model 2, oscillation 1)	19
Natural frequency of Dutch-roll lateral oscillation	20
Non-dimensional frequency parameter of lateral Dutch-roll oscillation	21
Phase relationships of Dutch-roll lateral oscillation	22(a-c)
Sample of data for determining damping of lateral Dutch-roll oscillation (model 2, oscillation 1)	23
Damping of Dutch-roll lateral oscillation	24
Amplitude ratios of Dutch-roll lateral oscillation	25(a-c)
Estimated values of n_p	26
Estimated values of ℓ_r	27
Vector diagram of Dutch-roll oscillation (model 2, oscillation 2)	28
Side-force derivative y_v	29(a-c)
Yawing moment derivative n_v	30(a-c)

LIST OF ILLUSTRATIONS (Contd)

	Fig.
Comparison of values of yawing moment derivative n_v between free-flight, wind-tunnels and estimates	31
Rolling moment due to sideslip derivative ℓ_v (model 2)	32
Roll damping derivative ℓ_p (model 2)	33
Yaw damping derivative n_r (model 2)	34
Side-force curves (models 2 and 3)	35(a,b)
Lift curves (model 3)	36
Sample of data for determining frequency of short period longitudinal oscillation (model 2, oscillation 1)	37
Natural frequency of short-period longitudinal oscillation	38
Non-dimensional frequency parameters of short-period longitudinal oscillation	39
Pitching moment derivative m_w	40
Lift force derivative z_w	41
Manoeuvre margin	42

1 INTRODUCTION

The Bristol T.188 is a single-seat aircraft, powered by two turbo-jet engines, which has been designed for aerodynamic and structural research at Mach numbers up to about 2.5. The general configuration is shown in Fig.1.

Although comprehensive wind-tunnel tests have been done on the design, free-flight tests were also considered necessary in order to obtain measurements free from the effects of wind-tunnel constraints. The 1/36th scale model tested in the R.A.E. Bedford 3 × 3 ft tunnel[1] had its afterbody considerably modified in order to accommodate the single-sting support and the 1/12th scale model tested in the R.A.E. Bedford 8 × 8 ft supersonic tunnel[2,3] and the A.R.A. 9 ft × 8 ft transonic tunnel[4] was supported on twin stings running into the rear of the engine nacelles.

The present paper describes a series of experiments conducted to investigate the lateral stability of the design and in particular to measure the stability derivative n_v at the higher Mach numbers. This is of special concern because the destabilising contributions to n_v from the long forebody and nacelles remain fairly constant with increasing Mach number while the stabilising effectiveness of the fin decreases with Mach number so that a rather fine balance of large moments may exist at the upper end of the speed range with the attendant risk of poor lateral behaviour.

The lateral-stability analysis of the free-flight tests was based on the Dutch-roll oscillation and was therefore complicated by the presence of three degrees of freedom, sideslip, yaw and roll, compared with, say, the more simple analysis of longitudinal stability involving two degrees of freedom only. Very little free-flight model work has been done in this country on the lateral-stability problem; therefore the present investigation was started rather tentatively with simplified models and instrumentation. Because of this, some of the results from the first two models in the series are not applicable to the full-scale aircraft but they are included here because of their interest in terms of technique development. The third model was more representative of the full-scale aircraft though differing from the true configuration by having slightly modified body lines and trapezoidal, instead of circular-arc, wing sections. These differences, however, are expected to have only very small effects on the lateral-stability characteristics and the model yielded reliable stability data from which useful comparisons with the wind-tunnel results have been deduced.

Although the aerodynamic results from this investigation may be of somewhat limited interest, being applicable to this particular aircraft only, they do show, when compared with the wind-tunnel results, how important the effects of sting supports can be. From the point of view of free-flight testing, the programme has provided a valuable opportunity for examining the suitability of several different, and in some measure independent, methods of lateral-stability analysis. Vector methods and analytic methods have yielded consistent results and the effects of various approximations to the complete Dutch-roll analysis have been investigated.

2 DESCRIPTION OF THE MODELS

All three models were to 1/12 scale and are illustrated in Figs.2-8; their principal data are listed in Table 1. They were simplified for ease of production by having the aerofoil sections modified from circular arc to trapezoidal sections and the bodies reduced to circular cross-sections about a straight centre-line. Some refinements to this simple layout were made on model 3 as described later. Wings and tail surfaces were machined from solid aluminium-alloy and the bodies were fabricated from aluminium-alloy tube with

brass and magnesium castings for the nose and tail portions respectively. To minimise the effects of aero-elastic distortion particular care was taken in the design and manufacture of the body joints to make them rigid. The nacelles of models 1 and 2 were made from standard aluminium alloy tube to give an approximate representation of the nacelle design current at that time. This has since been superseded.

Models 1 and 2 were identical apart from small differences in c.g. position and moments of inertia, and the presence of the incidence/yaw probe on the nose of the second model. No provision had been made on the first model for the deliberate excitation of the lateral oscillation but the second and third models were equipped with 5 lateral thrust units, 'bonkers', mounted in the tail cone and timed to fire at 1 second intervals after the model had separated from its boost motor. The positions of the bonkers are given in Figs.2 and 3 and a photograph of the installation is given in Fig.4(d).

The third model was intended to repeat the experiment made with model 2 but with the main features of the aircraft that were expected to effect the lateral stability more accurately represented. These were considered to be the body side elevation, the fin aerofoil section and planform and the nacelles. The body profiles of the models are compared with the full-scale aircraft in Fig.5. The small side-area of the first two models is clearly apparent, this was remedied on the third model by building up the body with a wooden fairing to represent the cabin and, approximately, the centre-line profile of the fuselage. The body camber was not represented since this could not be achieved by any simple modification to the basic body and, in any case, was not thought likely to have much effect on the lateral stability. The moderate amount of body waisting on the actual aircraft was not represented.

Details of the fin as used on the first two models are given in Fig.7(a). These were relatively crude representations of the aircraft fin and the results from the second model strongly suggested that the fin suffered considerable loss of effectiveness below M = 1.8, possibly arising from flow separation at the forward ridge line which is nearly sonic at this Mach number. The fin for the third model was therefore made to the correct planform and the forward ridge line was removed by building up the aerofoil section with an araldite fairing (Fig.7 b). The aft ridge-line was also removed by working it down to a smooth curve. The engine nacelles on model 3 were the same as those on the wind-tunnel models[1,2,3,4] and represented the nacelle design for the Gyron Junior installation to be flown on the first full-scale aircraft. The free-flight model nacelles were designed to have their exits choked to give full mass flow at the intake at M = 2.0; details are given in Fig.8. Each nacelle housed a magnesium flare to aid visual tracking by kinetheodolites and high speed cameras.

The telemetry equipment carried by each model is summarised in Table 2. The most important measurements required for the lateral stability analysis are the angular rates (or angular accelerations) about the yawing and rolling axes, the lateral acceleration at the c.g. and the angle of sideslip. The models were too small to accommodate existing rate gyroscopes or angular accelerometers and so the necessary angular acceleration data had to be obtained from linear accelerometers suitably disposed about the appropriate axes. The angular acceleration in yaw was obtained from two lateral accelerometers mounted in the body, one near the c.g. and one in the tail, and rolling acceleration was obtained from normal accelerometers mounted inside the centre body of each nacelle. The two normal accelerometers in the fuselage were used for the longitudinal stability analysis.

Model 1 carried a transponder-Doppler unit to measure velocity but this could not be installed in the later models because of lack of space and so their velocities had to be derived from kinetheodolite data only. The models were accelerated to their maximum velocity of about 3000 ft/sec by a single solid fuel motor. They were mounted in the pick-a-back position as shown in Fig.4(e) and separated from the boost motor automatically at all-burnt.

3 FLIGHT BEHAVIOUR

Trajectory, velocity and Mach number curves for all three models are given in Figs.9, 10 and 11. The small increases in maximum velocity on the second and third models were achieved by keeping the model/boost combination as clean and light as possible. For reasons of range safety the models were required to roll at about one revolution per second throughout their flight; this was to ensure that they would keep within the desired safety area should they fly at a high lift coefficient. The roll was obtained by setting a differential incidence of 10 minutes between the two wing panels. The rates of roll are plotted in Fig.13 which shows that the first two models rolled at about the desired rate over the larger part of their flight but that the third model rolled at a higher rate at the higher Mach numbers. The main effect of the steady rate of roll on the lateral behaviour arises from inertia cross-coupling and the yawing moment derivative n_p so as to induce a steady angle of sideslip. The magnitude of the sideslip angle was, however, always small because the roll frequency was kept well below the yaw and pitch frequencies so that roll-pitch-yaw divergence could not occur. The way in which the side-force and sideslip follow the superimposed rate of roll can be seen most clearly on model 3 at the higher Mach numbers (Figs.13,14,15). The effect of the steady rolling motion on the lateral oscillatory mode should appear in the form of a perturbation at the frequency of the short period longitudinal oscillation. Close examination of the lateral oscillatory data failed to show any such effect and so the superimposed rate of roll was neglected in the analysis for the lateral stability derivatives.

Curves of mean lift coefficient and incidence are given in Figs.16 and 17. The values of the mean lift coefficient for models 1 and 3 agree very closely and follow the trend of decreasing $C_{L_{mean}}$ with increasing Mach number expected from the results of wind-tunnel tests. The behaviour of model 2, however, was quite different in that the mean lift coefficient decreased in several distinct steps as the velocity fell, finally trimming out at a small negative C_L at subsonic velocities. The most likely explanation for this is that the tailplane on this model suffered some loss of effectiveness because of local flow separations over the fin, particularly at the higher angles of yaw at the beginning of each oscillation. The basis for this argument is given more fully in Section 5. The only oscillation that could be analysed on the first model for the evaluation of the stability derivatives was that produced by the disturbance as the model separated from the boost motor. On the second model the separation oscillation was analysed and four of the five bonker-excited oscillations; one was of too small amplitude for accurate measurement. On the third model all five bonker oscillations and the separation oscillation were analysed. A sample of the telemetry record is shown in Fig.18. Unfortunately on this model the two normal accelerometers in the nacelles, which were needed to obtain the oscillatory roll data, failed at the moment of separation.

4 METHODS OF ANALYSIS

4.1 Basic principles

For the analysis of the stability measurements the flight of each model was broken down into a number of discrete time intervals during each of which the velocity was assumed constant. These intervals generally corresponded to the duration of the oscillation between the firing of one bonker and the next, but some oscillations were subdivided and analysed over two intervals where there was a measurable change in the frequency of damping characteristics.

The analysis was based on the classical equations of aircraft dynamic stability but only five degrees of freedom were considered because of the constant-velocity assumption. It was also assumed that the second-order terms of the perturbation velocities were negligible and that there was no aerodynamic cross-coupling between the longitudinal and lateral modes. Body axes were used with the x axis along the body centre-line and all instruments were accurately aligned with this set of axes.

The equations of motion then reduce to

(a) The longitudinal set

$$\hat{t}\left(\frac{\dot{w}}{V} - q\right) + \frac{1}{2} C_L(1 - \cos\varphi) - z_w \frac{w}{V} = 0 \qquad (1)$$

$$\hat{t}\, i_B \dot{q} \frac{\bar{c}}{V} - m_w \frac{w}{V} - m_q q \frac{\bar{c}}{V} - m_{\dot{w}} \frac{\dot{w}}{V^2} \bar{c} = 0 . \qquad (2)$$

(b) The lateral set

$$\hat{t}\left(\frac{\dot{v}}{V} + r\right) - \frac{1}{2} C_L \varphi - y_v \frac{v}{V} = 0 \qquad (3)$$

$$\hat{t}\left(i_A \dot{p} \frac{b}{2V} - i_E \dot{r} \frac{b}{2V}\right) - \ell_p p \frac{b}{2V} - \ell_r r \frac{b}{2V} - \ell_v \frac{v}{V} = 0 \qquad (4)$$

$$\hat{t}\left(i_C \dot{r} \frac{b}{2V} - i_E \dot{p} \frac{b}{2V}\right) - n_p p \frac{b}{2V} - n_r r \frac{b}{2V} - n_v \frac{v}{V} = 0 . \qquad (5)$$

Because of the complicated motion about all axes experienced by the models, as illustrated by the telemetry record (Fig.18), the use of these simplified equations requires some comment.

The primary object of the experimental programme was to measure the yawing-moment derivative n_v, and with the instrumentation available this was considered feasible since n_v is one of the dominant derivatives determining the frequency of the Dutch-roll oscillation. Considering the aircraft configuration one would not expect large aerodynamic coupling derivatives from the longitudinal into the lateral mode because of the moderate sweep, lack

of dihedral, and attached-flow conditions that should exist over the wing for the very low incidence range covered by the tests. For example, wind-tunnel tests[1] have shown that at M = 2 the variations of n_v and ℓ_v with incidence are less than ±5% for the free-flight model conditions.

The assumption that the lateral motion is independent of the longitudinal oscillation looks reasonable in the first instance from examination of the lateral-accelerometer and sideslip records of Fig.18. The lateral motion appears to be a simple damped harmonic oscillation practically unaffected by the higher-frequency oscillation in the pitch-plane. This is confirmed in that independent methods of analysing the lateral motion based on these simplifying assumptions give consistent and reasonable results. On the other hand the pitching motion is evidently strongly influenced by the lateral oscillation so that the wave-form is composed of at least two superimposed oscillations and the amplitude is not exponentially damped in fact; it increases for the first few cycles. Standard methods of analysis for the longitudinal-stability data cannot, therefore, be applied, and only approximate values of m_w and z_w have been obtained. But, since the main emphasis of the investigation was on lateral stability, a more detailed analysis of the longitudinal motion was not considered justified. In the following paragraphs several methods of lateral-stability analysis are described. These have all been applied to the present tests for the following reasons:-

(a) Some practical experience was required on the suitability of the various methods of analysis for free-flight testing.

(b) The effects of various degrees of approximation had to be investigated, particularly because of the incomplete data recorded from the third model.

4.2 Lateral stability

4.2.1 Analytic solution (method A)

The instrumentation system yields direct measurements of linear acceleration at various points on the model, angle of incidence and sideslip. The various methods of analysis adopted to extract the aerodynamic derivatives require this data in the following form:-

(a) Frequency and damping of the Dutch-roll oscillation.

(b) Amplitude relationships between roll, yaw and sideslip.

(c) Phase relationships between roll, yaw and sideslip.

(d) Continuous curves of side-force and sideslip for two or three cycles of each oscillation.

The angular acceleration in yaw was obtained from the two lateral accelerometers and the roll acceleration from the two normal accelerometers in the nacelles. This latter pair of instruments was also responding to the longitudinal oscillation and so the quality of the data for determining roll acceleration was not so good as that for the yaw acceleration.

A sample of the data for determining frequency and phase angle is given in Fig.19 and the collected frequency data from all the models are plotted in Fig.20 and again in Fig.21 in the form of the non-dimensional lateral-frequency parameter. Phase relationships for model 2 are presented in Fig.22. The quality of the roll data relevant to the oscillations at M = 1.55 and 1.9

was such that the phase comparisons, $\phi_{\dot{p}\dot{r}}$, at these Mach numbers were considered unreliable and values from the mean curve were taken and used in the analysis. The damping of the Dutch-roll oscillation was obtained by drawing the best set of parallel lines through the log-plots of the yawing and rolling accelerations and the sideslip angles. A sample of these plots is given in Fig.23 and the collected damping results are plotted in Fig.24. The amplitude ratios between the three degrees of freedom of the Dutch-roll oscillation were obtained from the logarithmic damping plots of the kind shown in Fig.23.

Voepel[5] has shown that the lateral set of equations (3), (4), (5) can be solved in terms of the amplitude and phase relationships of roll, yaw and sideslip to yield the following expressions for the more important derivatives.

$$n_v \simeq \frac{i_C}{\mu_2}\left(\hat{t}\,\frac{K_{\dot{r}}}{K_{\dot{\beta}}}\right)^2 \left\{\frac{1 - e_C \left|\frac{K_{\dot{p}}}{K_{\dot{r}}}\right| [\text{sg. cos } \phi_{\dot{r}\dot{p}}]}{1 - e_A\, e_C}\right\} \tag{6}$$

$$\ell_v \simeq \frac{i_A}{\mu_2}\left(\hat{t}\,\frac{K_{\dot{r}}}{K_{\dot{\beta}}}\right)^2 \left\{\frac{\left|\frac{K_{\dot{p}}}{K_{\dot{r}}}\right| [\text{sg. cos } \phi_{\dot{r}\dot{p}}] - e_A}{1 - e_A\, e_C}\right\} \tag{7}$$

$$y_v \simeq g\,\frac{\hat{t}}{V}\,\frac{K_{ay}}{K_{\beta}} \tag{8}$$

where sg. cos ϕ is the sign of the trigonometrical function. In the figures the results from these expressions are labelled 'method A'. They have been obtained for model 2 only because of the lack of roll information from the other models.

4.2.2 Vector solution (method B)

The vector method of analysis for oscillatory damped motions, due to Doetsch[6], has been applied to the rolling and yawing-moment equations (4) and (5). While, in principle, the vector solution should give the same answers as the analytic solution (method A), the experimental data is used somewhat differently in each case so that different experimental errors may arise. These considerations are discussed more fully in para 5.1.

If the Dutch-roll mode only of the lateral motion is considered, then the variables p, r and β in equations (4) and (5) may be considered as vector quantities all having the same period and damping. The measured quantities were actually angular accelerations $\dot{p}$ and $\dot{r}$ and the sideslip angle β but the corresponding amplitude and phase data for the rates can be obtained from the known relationships between rate and acceleration vectors in a damped harmonic system. Namely:

(a) The undamped natural frequency gives the amplitude ratio between the acceleration and rate vectors so that

$$\left|\frac{K_{\dot{p}}}{K_p}\right| = \left|\frac{K_{\dot{r}}}{K_r}\right| = \left|\frac{K_{\dot{\beta}}}{K_\beta}\right| = \omega_n \quad .$$

(b) The acceleration vector leads the velocity vector in phase by 90° plus the damping angle, so that

$$\phi_{\dot{p}p} = \phi_{\dot{r}r} = \phi_{\dot{\beta}\beta} = 90^\circ + \varepsilon_D$$

where

$$\text{Tan } \varepsilon_D = \frac{\lambda}{\omega} \quad .$$

Although sideslip measurements were available from the yawmeter probe, they were not used in the vector analysis because the acoustic lags in the piping between the sensing head and the transducers precluded accurate evaluation of the sideslip phase relationship. More consistent results were obtained by using the lateral acceleration at the centre of gravity and vectorially solving for β by the kinematic relationship.

$$a_y - \frac{V}{g}(\dot{\beta} + r) + \varphi = 0 \quad . \qquad (9)$$

Sample vector solutions from model 2 for equations (4), (5) and (9) are given in Fig.28. In both the yawing and rolling moment polygons there are three unknown derivatives so that a solution is not possible unless one derivative in each case is known or assumed. In the present analysis the yawing and rolling moment derivatives exercising the least influence on the Dutch-roll oscillation were n_p and ℓ_r respectively and estimated values of these were used (Figs.26 and 27). This complete form of the vector analysis of the Dutch-roll motion yields data on n_v, n_v, ℓ_v and ℓ_p. It has been applied to the measurements from model 2 only, because of the lack of roll information from the other models, and in the figures is referred to as "VECTOR METHOD B".

4.2.3 Simplified solutions (methods C,D,E)

The lack of roll measurements for models 1 and 3, and sideslip data for model 1, precludes the complete analysis of their lateral-stability characteristics by the previous two methods A and B. Therefore various simplified methods have had to be applied.

Analytic solution (method C)

The crudest approach is to neglect the freedom in roll altogether so that the Dutch-roll mode is simplified to a two-degree-of-freedom oscillation in yaw and sideslip. The solution is then analogous to that for the short-period oscillation in the longitudinal mode[7] and yields a value for n_v depending on the frequency only of the lateral oscillation so that,

$$n_v \simeq \frac{i_C}{\mu_2}\left(\omega_{n_2}\hat{t}\right)^2 \qquad (10)$$

Also the focal-point analysis[7] can be used to give

$$y_v \simeq \omega_{n_2}^2 \frac{\hat{t}}{V} D \quad . \tag{11}$$

Analytic solution (method D)

A closer approximation for n_v has been derived by Thomas and Neumark[8] which includes the yawing-moment term arising from the rolling derivative ℓ_v and the product of inertia. Then,

$$n_v \simeq \frac{i_C}{\mu_2}\left(\omega_{n_2} \hat{t}\right)^2 - \ell_v \frac{i_E}{i_A} \quad . \tag{12}$$

Vector solution (method E)

A simplified vector solution can be obtained by neglecting the rolling motion; this should produce an answer for n_v corresponding to that of equation (10) (method C). This approximation is shown by the dotted line on the vector diagram for the yawing-moment equation (Fig.28). In this figure the resulting error in n_v is clearly apparent and, in this instance, arises mainly from neglecting the product of inertia term. The effect of neglecting the yawing-moment derivative n_p is very small.

4.2.4 Direct solution for y_v (method F)

The previous two methods for obtaining y_v, equation (8) (method A) and equation (11) (method C) use data from the envelopes only of the lateral oscillation. They therefore give average values of y_v over the range of sideslip covered and do not yield any information on the linearity of the side-force coefficient with sideslip. It is possible to plot side-force curves directly from the records of the lateral accelerometer at the c.g. and the sideslip probe. These are shown for models 2 and 3 in Fig.35.

4.3 Longitudinal stability

Because of the complex motion in the longitudinal mode the only derivatives that could be extracted with reasonable confidence were z_w and m_w. Lift curves were obtained from model 3 from the data yielded by the normal accelerometer at the c.g. and the incidence probe (Fig.36). These were considered linear within the experimental accuracy and the slopes are plotted as z_w against Mach number in Fig.41.

It was possible to extract the frequency of the pitching oscillation for all models. A typical frequency plot is shown in Fig.37 and the collected frequency information from all three models is given in Figs.38 and 39. In the usual analysis[7] of the short-period longitudinal oscillation the pitching moment derivative m_w is obtained from the approximate relationship

$$m_w \simeq \frac{i_B}{\mu_1}\left(\omega_{n_1} \hat{t}\right)^2 \quad . \tag{13}$$

In the present experiment, because the damping could not be evaluated, the measured pitch frequency ω_1 was used in place of the undamped value ω_{n_1}. This should, however have only a small effect on the evaluation of m_w.

4.4 Corrections for centre of gravity shift

The centre of gravity positions on the free-flight models were brought forward compared with the full-scale aircraft in order to obtain the relatively high frequencies of the oscillatory modes required for analysis. The measured values of the moment derivatives have therefore had to be corrected to make them comparable with the wind tunnel results and theoretical estimates.

A corrected curve for n_v is given in Fig.31 where

$$n_{v_F} = n_{v_M} - \frac{y_v}{b/2}\left(x_{c.g._M} - x_{c.g._F}\right) . \qquad (14)$$

The suffices F and M refer to the values appropriate to the full-scale and model centre of gravity positions respectively. The values of y_v used in this expression were those measured on the appropriate model, i.e. from Fig.29(b) for model 3.

Corrected curves for m_w are given in Fig.40(b) where

$$m_{w_F} = m_{w_M} - \frac{z_w}{\bar{c}}\left(x_{c.g._M} - x_{c.g._F}\right) . \qquad (15)$$

5 DISCUSSION OF RESULTS

5.1 Lateral stability

The very limited data obtained from model 1 showed that while the longitudinal stability characteristics were in fair agreement with estimates (Figs.40 and 41) the lateral stability derivative n_v appeared low. The second model yielded results that agreed with those from the first one at M = 2.4 and because of the more comprehensive instrumentation enabled a full analysis to be made of the Dutch-roll oscillation. Furthermore, the 'bonker' installation allowed the stability to be investigated over the Mach number range 1.2 to 2.5. The third model was much more representative of the full-scale configuration but unfortunately a full analysis of the lateral motion could not be made because of the failure of the roll accelerometers. This was not, however, so serious as might be supposed because careful comparison of the results from various methods of analysis for each model has given a good measure of the effect of the rolling freedom on the yawing motion.

Since the main purpose of the investigation was to obtain values of n_v, the discussion will be mainly concerned with the evaluation of this derivative with only a few remarks on the other information obtained.

In Fig.30 the results from the five methods of analysis for n_v are compared for model 2. The simplest solutions, methods C and E (Fig.30a)

which neglect the freedom in roll completely, yield results which are in close agreement with each other. Theoretically, of course, they are bound to agree since they are merely two ways of solving the same equations. In their practical application to experimental data, however, the same result will only be obtained if the instrumentation system is working satisfactorily since method C depends upon the frequency only of the lateral oscillation whereas the simplified vector solution E uses amplitude and phase measurements from the motions in yaw and sideslip. The measure of agreement between these two solutions is therefore a useful guide to the accuracy of the instrumentation system.

The two methods A and B, which include the rolling freedom, also yield results which are in close agreement with each other (Fig.30b) but the general level of the n_v curve is about 10% higher than that obtained from the simple solutions C and E. This difference arises from neglecting the terms $-n_p \cdot \frac{pb}{2V}$ and $-i_E \hat{t} \frac{\dot{p}b}{2V}$ in the simplified solutions. The vector diagram for the yawing motion (Fig.28) shows clearly that, in this instance, it is the product of inertia term which plays the more important part. The approximate solution D (Fig.30b), which neglects all the rolling terms except for the derivative ℓ_v and its coupling into the yawing moment via the product of inertia i_E, yields results for n_v which are in very close agreement with those from the more complete forms of analysis (methods A and B). The fact that only the ℓ_v term is necessary to give a close approximation to the result from the complete solution is most useful and has been used in the analysis of the third-model results.

The most surprising feature of the n_v curves from model 2 was that the values of n_v increased with increasing Mach number instead of decreasing as the estimated values suggest. This was thought to be a most unlikely characteristic of the design and an explanation was sought by examination of the other aerodynamic characteristics of the model. The main clues are evident in Figs.29(a) and 40, which indicate that a change in aerodynamic characteristics occurred near M = 2. As the Mach number fell below this value the longitudinal stability suddenly decreased and there was also a fairly sudden loss of y_v. The major contribution to m_w arises from the tailplane, and a large proportion of y_v from the fin. Thus the whole tail assembly appears to have suffered a considerable loss of effectiveness below M = 2.0. The most probable cause of such a loss was thought to be a flow separation from the forward ridge line on the fin. Such a separation is most likely to occur when the component of the local flow normal to the ridge-line falls to a subsonic value. The geometry of the fin (Fig.7a) is such that this corresponds to a flight Mach number of about 1.8. A complete flow separation from this line would cause a marked loss of effectiveness of the fin and also of the tailplane because of its position above the fin. Although there was no direct proof that this explanation was the correct one, it seemed plausible enough to justify a modification to the fin of the third model which would eliminate the offending ridge lines. At the same time the fin shape was altered to make it more representative of the full-scale fin (Fig.7b).

The effects of the fin modifications on the lateral and longitudinal characteristics is evident from comparison between the results of the second and third models in Figs.29, 30 and 40. There were other differences between the second and third models, notably in the fuselage cross-section and the nacelle size as mentioned earlier, but it is unlikely that these caused the marked difference in characteristics below M = 2.0. At Mach numbers above 2.0 the results from the second and third models are in good agreement.

The values of n_v for the third model are given in Fig.30(c). They have been calculated from the lateral-frequency data (method C) and from the better approximation of method D. Since a complete lateral analysis was not possible on this model no measured values of ℓ_v were obtained for substitution in the equation of method D. The values actually used are given in Fig.32. Here the measured values from the second model show the same drop below M = 2 as occurred in the other derivatives mainly dependent on tail effectiveness. But since the third model did not suffer from this trouble, an estimated curve for ℓ_v has been used which agrees fairly well with the measured values from model 2 around M = 2.0

Admittedly, the ℓ_v data of Fig.32 may not be very accurate but even a 25% error in the values of ℓ_v used in method D does not effect the values of n_v by more than 5%.

The n_v curve from model 3 has been corrected to the full-scale centre of gravity position and is presented in Fig.31 in comparison with the estimated curve and the wind-tunnel results from Refs.1-4. Between M = 1.4 and 2.0 the results from the free-flight model and the 8 × 8 ft tunnel are in good agreement but above M = 2.0 the free-flight result falls below the tunnel values until at M = 2.4 there is a discrepancy of 20% in n_v. In general the curve from model 3 follows the trend of the estimated values but lies some 10% - 20% below them. Near M = 1.4 the results from the free-flight model, the 8 × 8 ft tunnel, the 9 × 8 ft tunnel and the estimated values all lie close together. The results from the 3 × 3 ft tunnel model are some 40% too high throughout the Mach number range of the tests. This is perhaps not surprising in view of the modifications made to the afterbody of the model.

Some confidence may be placed in the accuracy of the free-flight results for n_v since the evaluation of this derivative is mainly dependent on the yawing frequency which can be measured to an accuracy of about ±3%. The uncertainty in the value of ℓ_v has been shown to have only a small effect and a pessimistic evaluation of all the experimental errors in the free-flight analysis indicates that the overall accuracy of n_v should be within ±10%. The curve for model 3 on Fig.31 may therefore be taken as a fairly accurate measurement of n_v on the <u>free-flight model</u> when measured in the <u>oscillatory mode</u>.

The question then arises as to how closely the model represents the full-scale aircraft configuration (Figs.1 and 3). The major geometrical differences, as discussed in Section 2.0 were introduced to simplify the model construction and are considered to have only a very small effect on n_v. The most significant difference between the aerodynamics of the free-flight models and the full-scale aircraft lies in the possible effects of the efflux from the engines on the flow field around the tail assembly. The internal flow through the model nacelles is not fully expanded as it leaves the nacelle exit. The nacelles were designed to have sonic flow at the exit giving a pressure ratio, between the internal and external flows at the exit, of 3.8 at M = 2.0. There will, then, be some local shock pattern arising from the expansion of the internal flows as they leave the nacelle exits, which will impinge on the fin and tailplane at certain Mach numbers. No attempt has been made in the present analysis to assess the significance, in terms of lateral stability, of the differences between this (model) flow and the engine efflux on the full-scale aircraft. Some aspects of this flow interference problem have been investigated in the Bedford 3 × 3 ft supersonic wind-tunnel.

Turning now to the discussion of the other lateral derivatives, the most reliable results were obtained for y_v. Here again several methods of analysis have been applied which yield fairly consistent results. The curves of C_y against β (Fig.35) for model 3 are linear within the experimental accuracy over the range of sideslip covered but there is some evidence of non linearity in the results from model 2. The suspected reason for the loss of y_v on model 2 below M = 2.0 has already been discussed in Section 5 and has been ascribed to flow separation from the forward ridge line of the fin. The curve of Fig.29(a) cannot therefore be considered representative of the full-scale aircraft. In Fig.29(c) the values of y_v obtained from model 3 (Fig.29b) are compared with the wind-tunnel results and theoretical estimates. There is again close agreement between the results from the free-flight model and the 8 x 8 ft and 9 x 8 ft wind-tunnel model except above M = 2.0 where, as in the case of n_v, the free-flight results start falling away below the wind-tunnel values. In this respect the y_v and n_v results are consistent.

The three derivatives ℓ_v, ℓ_p and n_r were obtained from model 2 only and are shown in Figs.32, 33 and 34. The values of ℓ_v were obtained from the analytic method A (equation 7) and the vector solution, method B. Here again the two approaches yield results which are in close agreement with each other and in fair agreement with the wind-tunnel values and estimated values at Mach numbers above 2.0.

The damping derivatives ℓ_p (Fig.33) and n_r (Fig.34) were obtained from the vector solution (method B). While there is fair agreement between the measured and estimated curves for ℓ_p, particularly in the variation with Mach number, there is a gross discrepancy between the measured and estimated values of n_r. Moving the centre of gravity aft from the model position ($-0.24\ \bar{c}$) to the full-scale position ($+0.18\ \bar{c}$) would reduce the measured values of n_r by some 15% only still leaving the larger part of the difference to be explained. The most likely reason for this discrepancy can be seen from the sample vector diagram (Fig.28) which is typical of all the diagrams obtained in the analysis of model 2. The amplitude ratios between the various components of the oscillatory motion, which give the length of the vectors, can generally be obtained to ±5% and the phase angles to about ±2°. While uncertainties of this order have only a small effect on the n_v vector and moderate effects on the ℓ_v and ℓ_p vectors, they clearly have a very large effect on the n_r vector. It is therefore not possible, with the instrumentation used on this model, to evaluate the n_r derivative with any reliability. For this reason no attempt has been made to correct the experimentally determined values to the full-scale c.g. position. It should be possible, however, with more accurate instrumentation to obtain n_r by free-flight techniques providing the derivative is large enough to influence the lateral oscillation by an appreciable amount.

5.2 Longitudinal stability

The experimental programme was mainly directed towards the investigation of lateral stability and the models were equipped accordingly. It was therefore something of a bonus that the laterally-mounted 'bonkers' also produced the large response in pitch evident in Fig.18. While a certain amount of the pitching motion was fed in from the lateral oscillation, a large

disturbance in pitch was clearly applied the moment each 'bonker' unit was fired. The reason for this is apparent from the location of the 'bonkers' in the tailcone (Figs.2,3 and 4d). A strong shock wave would form ahead of the bonker efflux being ejected from the body side so that the associated pressure field would react on the tailplane producing a nose-down pitching moment.

A full treatment of the longitudinal-stability analysis has not been attempted for the reasons given in Section 4.1.

The lift curves shown in Fig.36 cover only a very small range of incidence, $\pm 2^{\circ}$ at the most, but their slopes agree very well with the estimated values of z_w given in Fig.41. In spite of the complex nature of the pitching oscillation it was found possible to extract the short-period pitch frequency with a high degree of accuracy. The sample frequency-plot illustrated in Fig.37 is typical of all the oscillations and shows that the decreasing amplitude of the accompanying lateral motion has negligible effect on the frequency of the pitching oscillation. Some confidence can therefore be placed on the derived values of m_w as being appropriate to the pure pitching motion alone. The collected frequency data from all the models are presented in Fig.38 and again in Fig.39 as the non-dimensional frequency parameter $\omega_1 \bar{c}/V$.

The curves of the pitching moment derivative m_w (Fig.40a) clearly show the loss of stability on model 2 below M = 2 but the results from all the models, when corrected for the shift of centre-of-gravity, agree very closely with the estimated values above M = 2 (Fig.40b).

The manoeuvre margin has been evaluated from the relationship

$$-\frac{\partial C_m}{\partial C_L} = \frac{m_w}{z_w}$$

and has been plotted for all three models in Fig.42. Again there is close agreement between the measured and estimated values above M = 2 and reasonable agreement at lower Mach numbers for the third model.

6 CONCLUSIONS

(1) Several semi-independent methods of analysis have been applied to the lateral oscillatory mode of three free-flight dynamic-stability models and have yielded consistent results for the derivatives y_v, n_v, ℓ_v and ℓ_p. The methods have also shown the effect, on the evaluation of n_v, of neglecting the freedom in roll in the lateral motion.

(2) Comparison of these results with corresponding wind-tunnel tests have shown that, as measured on the most representative model, n_v was some 20% lower at M = 2.5 than values obtained in the Bedford 8 × 8 ft supersonic tunnel. At Mach numbers below 2 there was close agreement in n_v between the free-flight results and those obtained in the Bedford 8 × 8 ft and the A.R.A. 9 ft × 8 ft tunnels. Earlier measurements of n_v made on a small model with a large sting support in the Bedford 3 ft × 3 ft tunnel were some 40% higher than the free-flight results. Reliable data was also obtained on y_v which agreed closely with the 8 ft × 8 ft tunnel results up to M = 2.0 but were lower by about 10% at M = 2.4

From one of the models reasonable measurements of the derivatives ℓ_v and ℓ_p were obtained for Mach numbers between 1.8 and 2.4. At lower Mach numbers, however, this particular model is suspected of having suffered a severe loss of fin and tailplane effectiveness arising from a flow separation from a ridge line on the fin. The experimentally determined values of these derivatives below M = 1.8 are therefore probably unrepresentative of the full-scale aircraft on which such a flow separation should not occur.

(3) The longitudinal stability derivatives z_w and m_w were obtained for Mach numbers between 1.4 and 2.6 and these, in the main, agree well with the firm's estimates. They do not indicate any abnormal characteristics.

LIST OF SYMBOLS

A	inertia about roll axis
B	inertia about pitch axis
C_L	lift coefficient
C_m	pitching moment coefficient
C	inertia about yaw axis
D	distance of the focal point forward of the centre of gravity
E	product of inertia about the roll and yaw axes
K_{ay}	amplitude of lateral acceleration oscillation
K_β	amplitude of sideslip oscillation
K_p	amplitude of roll oscillation
K_r	amplitude of yaw oscillation
L_p	rolling moment due to rate of roll
L_r	rolling moment due to rate of yaw
L_v	rolling moment due to sideslip
M	pitching moment
M_w	pitching moment due to incidence
$M_{\dot{w}}$	pitching moment due to rate of change of incidence
M_q	pitching moment due to rate of pitch

N_p yawing moment due to rate of roll

N_r yawing moment due to rate of yaw

N_v yawing moment due to sideslip

S gross wing area

V flight-path velocity

W weight

Y_v side-force due to sideslip

Z_w normal force due to incidence

a_y lateral acceleration at the centre of gravity

b span

$\bar{c}$ geometric mean chord

$\bar{\bar{c}}$ aerodynamic mean chord

$e_A = i_E/i_A$

$e_C = i_E/i_C$

g acceleration due to gravity

$i_A = A/m\,(b/2)^2$

$i_B = B/m\,\bar{\bar{c}}^2$

$i_C = C/m\,(b/2)^2$

$i_E = E/m\,(b/2)^2$

$\ell_p = L_p/\rho S V\,(b/2)^2$

$\ell_r = L_r/\rho S V\,(b/2)^2$

$\ell_v = L_v/\rho S V\,(b/2)$

m = mass of model

$m_w = M_w/\rho S V\,\bar{\bar{c}}$

$m_{\dot{w}} = M_{\dot{w}}/\rho S\,\bar{\bar{c}}^2$

$m_q = M_q/\rho S V\bar{\bar{c}}^2$

$n_p = N_p/\rho S V (b/2)^2$

$n_r = N_r/\rho S V (b/2)^2$

$n_v = N_v/\rho S V (b/2)$

p rate of roll

q rate of pitch

r rate of yaw

$\hat{t} = m/\rho S V$

v lateral perturbation velocity

w normal perturbation velocity

x position of the centre-of-gravity along the body centre-line

$y_v = Y_v/\rho S V$

$z_w = Z_w/\rho S V$

α angle of incidence

β angle of sideslip

φ bank angle

ϕ phase angle (ϕ_{rp} is phase advance of r relative to p)

sg. cos ϕ sign of the cosine of ϕ

λ exponential index to the envelope of the damped oscillation

$\mu_1 = m/\rho S \bar{\bar{c}}$

$\mu_2 = m/\rho S (b/2)$

ν_1 frequency of short-period longitudinal oscillation

ν_2 frequency of Dutch-roll oscillation

$\omega_1 = 2\pi \nu_1$

$\omega_2 = 2\pi \nu_2$

ω_n undamped natural frequency

ρ air density

LIST OF REFERENCES

No.	Author(s)	Title, etc
1	Squire, L. C.	Wind-tunnel tests up to M = 2.0 on a model of the supersonic research aircraft E.R.134 (Bristol 188) R.A.E. Report Aero 2633, A.R.C.22 064. Dec. 1959.
2	Taylor, C. R., Cook, T. A.	Supersonic wind-tunnel tests on a 1/12th scale model of the Bristol type 188 research aircraft. Part 1. M = 1.4 to 2.0. R.A.E. Report Aero 2649, A.R.C.23 278. April 1961.
3	Cock, T. A.	Supersonic wind-tunnel tests on a 1/12th scale model of the Bristol type 188 research aircraft. Part 2. M = 2.0 to 2.7. R.A.E. Report Aero 2657, A.R.C.23 748. Sept. 1961.
4	Landon, R. H.	Transonic longitudinal and lateral stability tests and the effects of controls on a 1/12th scale model of the Bristol 188. Unpublished A.R.A. Note.
5	Voepel, H.	Unpublished M.O.A. Report.
6	Doetsch, K. H.	The time-vector method for stability investigations. A.R.C. R & M. 2945. August, 1953.
7	Hamilton, J. A., Hufton, P. A.	Free-flight techniques for high-speed aerodynamic research. Jour. Royal Aero. Soc. March 1956.
8	Thomas, H.H.B.M., Neumark, S.	Interim note on stability and response characteristics of supersonic aircraft. (Linear theory). R.A.E. Tech Note Aero 2412. A.R.C.18 263. November, 1955.

TABLE 1

Model data

	Model 1	Model 2	Model 3
Weight lb	113.3	107.7	117.3
Roll inertia (A) slug ft^2	0.418	0.390	0.450
i_A	0.0557	0.0549	0.0578
Pitch inertia (B) slug ft^2	6.56	6.46	6.808
i_B	1.768	1.831	1.772
Yaw inertia (C) slug ft^2	6.83	6.71	7.063
i_C	0.911	0.94	0.908
Product of inertia (E) slug ft^2	-	0.27	0.18
i_E	-	0.0380	0.0231
Relative density (mean) μ_1	556.8	559.5	591.8
μ_2	391.7	398.3	418.0
Centre of gravity	$-0.27\bar{c}$	$-0.24\bar{c}$	$-0.21\bar{c}$
Inclination of principal axis to datum axis	-	$-2^{\circ}27'$	$-1^{\circ}34'$

Wing area (gross)	2.75 ft^2
Aspect ratio	3.1
Geometric mean chord $\bar{c}$	0.94 ft
Aerodynamic mean chord $\bar{\bar{c}}$	1.027 ft
Semi-span b/2	1.462 ft

TABLE 2

Model instrumentation

465 Mc/s 24 channel telemetry

Model 1

±30g normal accelerometer 3.94 inches forward of c.g.
±30g " " 10.19 inches forward of c.g.
±30g " " 21.81 inches aft of c.g.
±7½g lateral accelerometer 3.94 inches forward of c.g.
0-10g longitudinal accelerometer 4.937 inches forward of c.g.

Transponder Doppler set.

Model 2

±10g normal accelerometer 2.00 inches forward of c.g.
±20g " " 17.56 inches aft of c.g.
±17½g " " in port nacelle
±17½g " " in starboard nacelle
±7½g lateral accelerometer 3.00 inches forward of c.g.
±10g lateral accelerometer 16.56 inches aft of c.g.
4 hole differential pressure hemispherical head for incidence and sideslip
5 Imp Mk.IV lateral thrust motors ('bonkers') timed to fire at 5,6,7,8,9 seconds after launch.

Model 3

±10g normal accelerometer 3.47 inches forward of c.g.
±20g " " 17.08 inches aft of c.g.
±17½g " " in port nacelle
±17½g " " in starboard nacelle
±7½g lateral accelerometer 2.37 inches forward of c.g.
±10g " " 15.98 inches aft of c.g.
4 hole differential pressure hemispherical head for incidence and sideslip
5 Imp Mk.IV lateral thrust motors timed to fire at 5.0, 6.2, 7.4, 8.6, 9.8 seconds after launch.

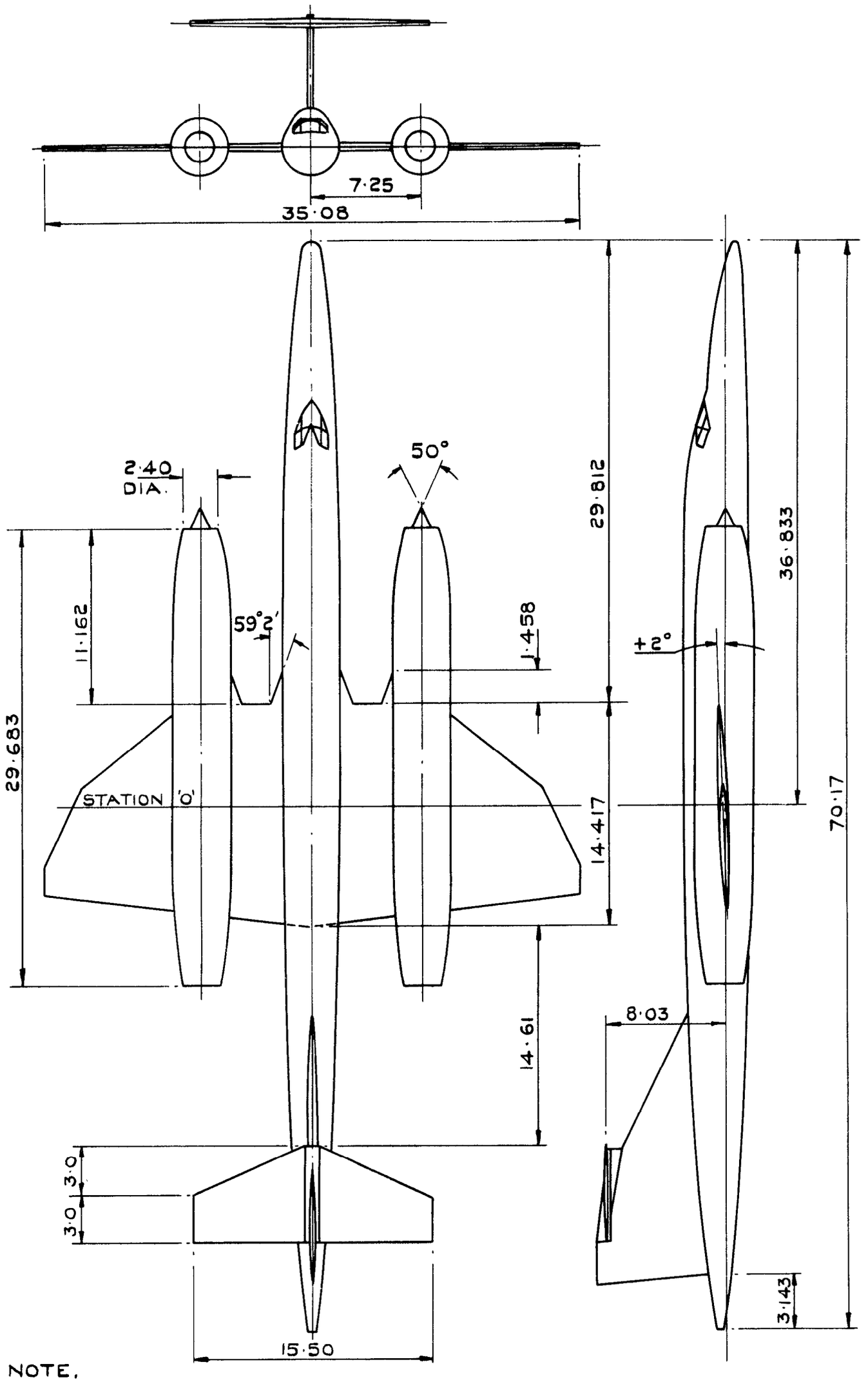

NOTE,
DIMENSIONS IN FEET.

FIG. 1. THE FULL-SCALE AIRCRAFT.

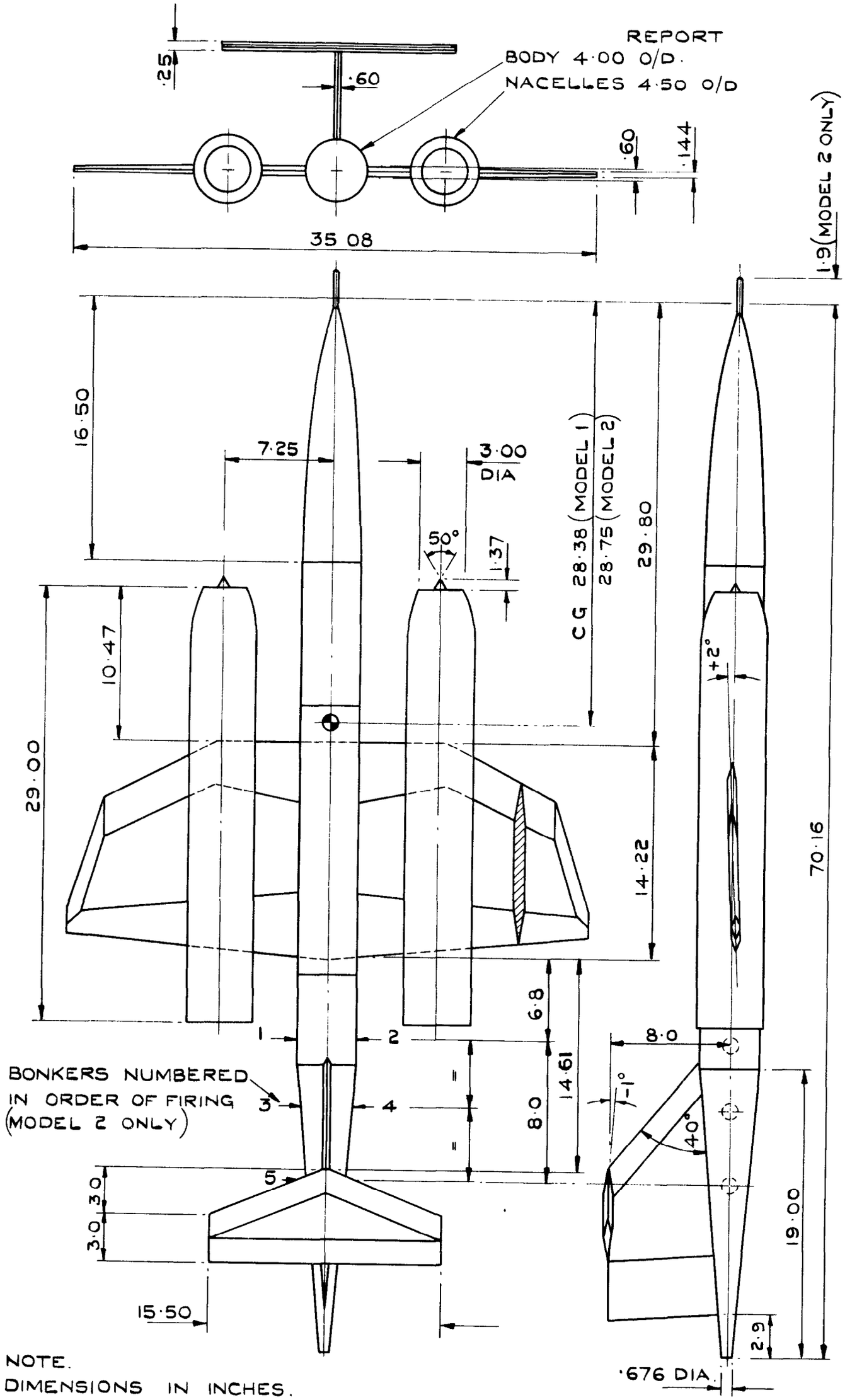

NOTE.
DIMENSIONS IN INCHES.

FIG.2. GENERAL ARRANGEMENT OF MODELS 1 & 2.

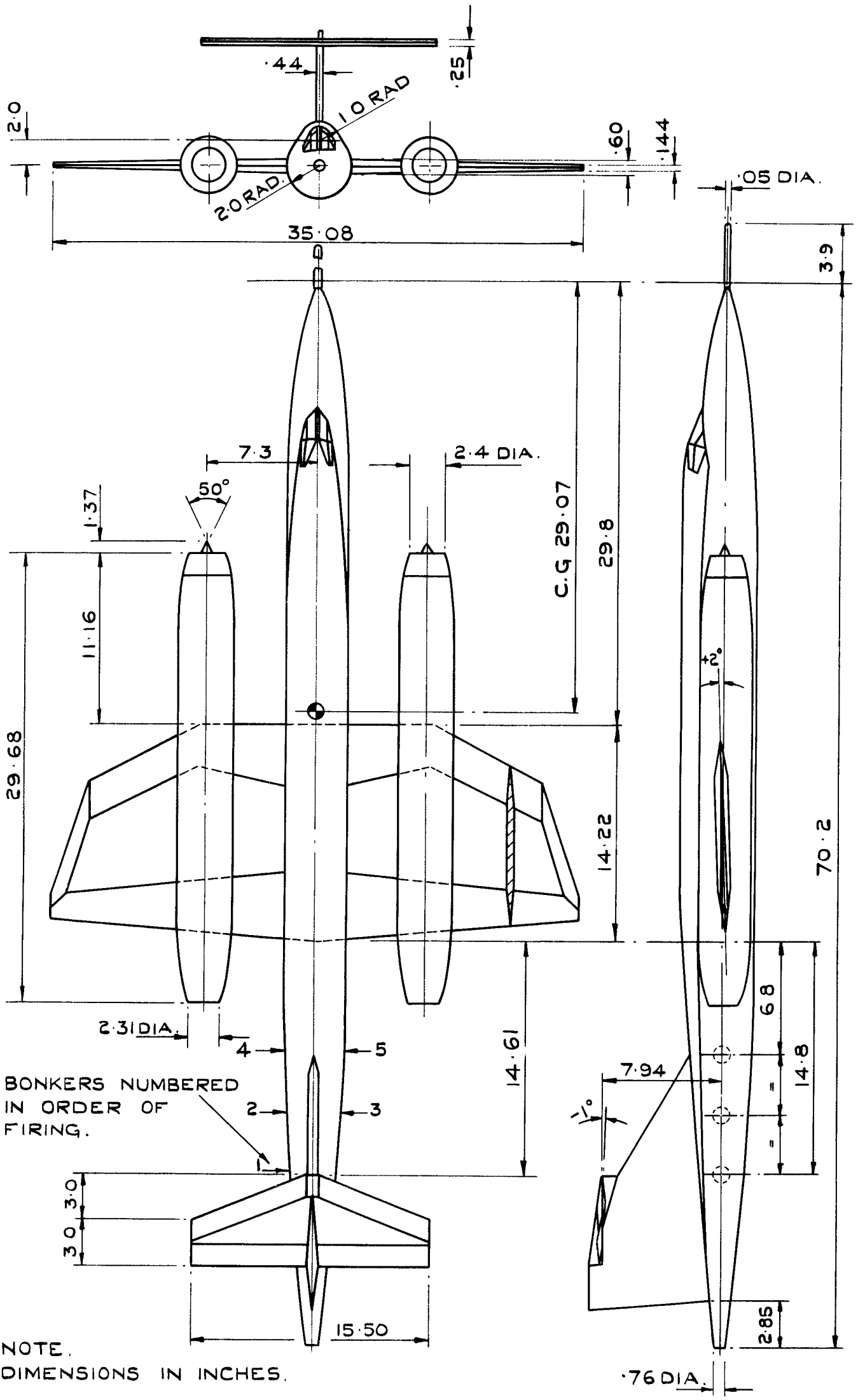

FIG. 3. GENERAL ARRANGEMENT OF MODEL 3.

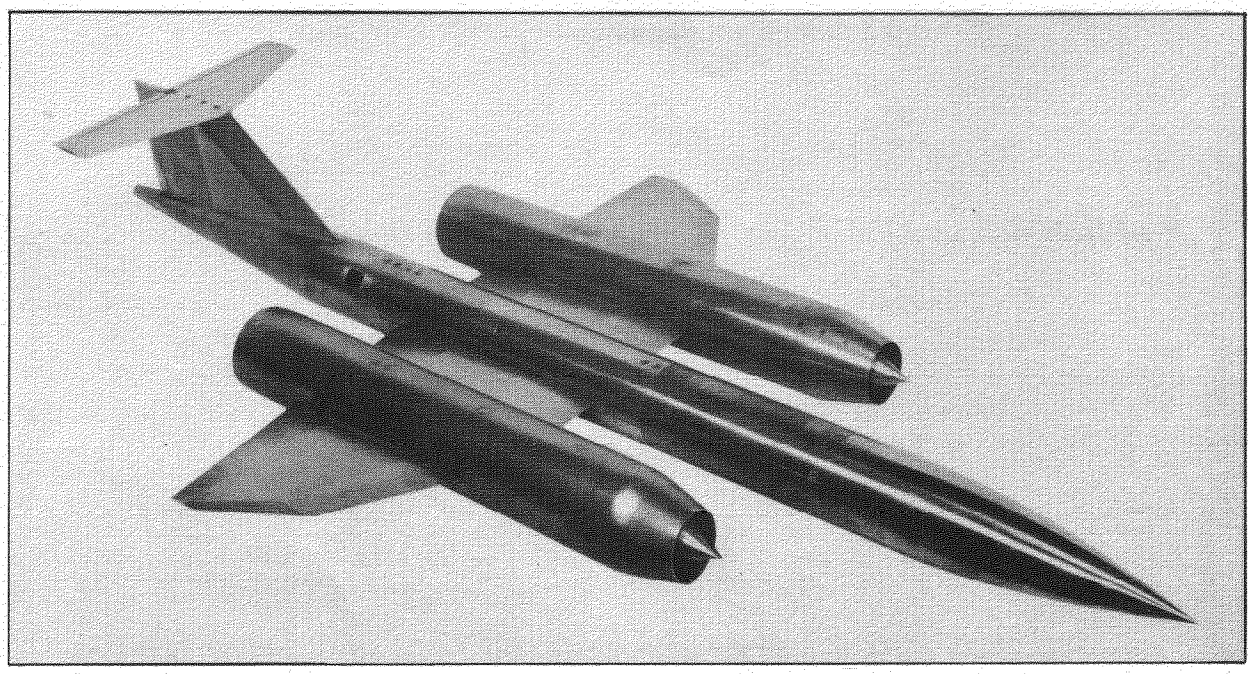

a. MODEL 1

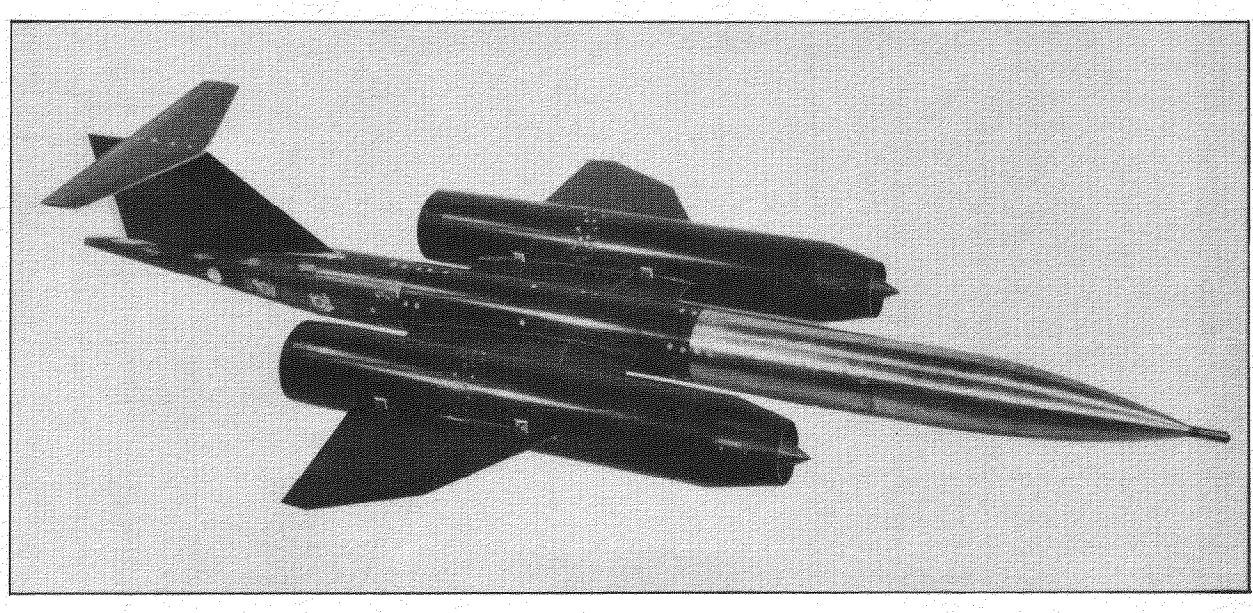

b. MODEL 2

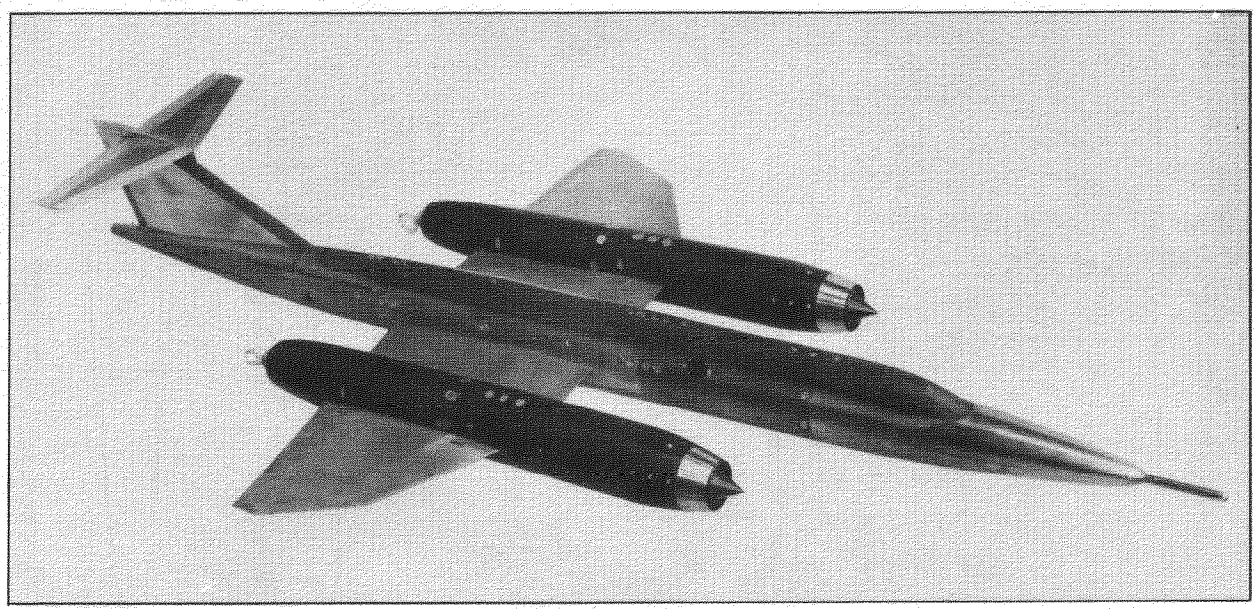

c. MODEL 3

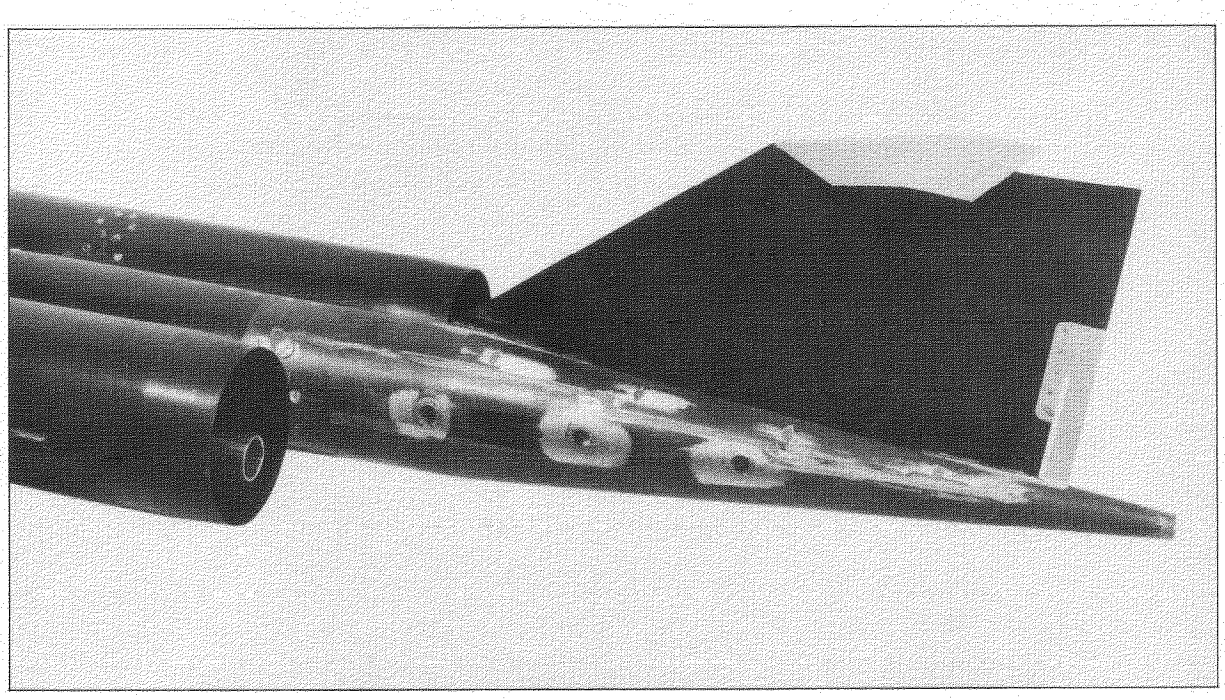

d. BONKER INSTALLATION MODEL 2

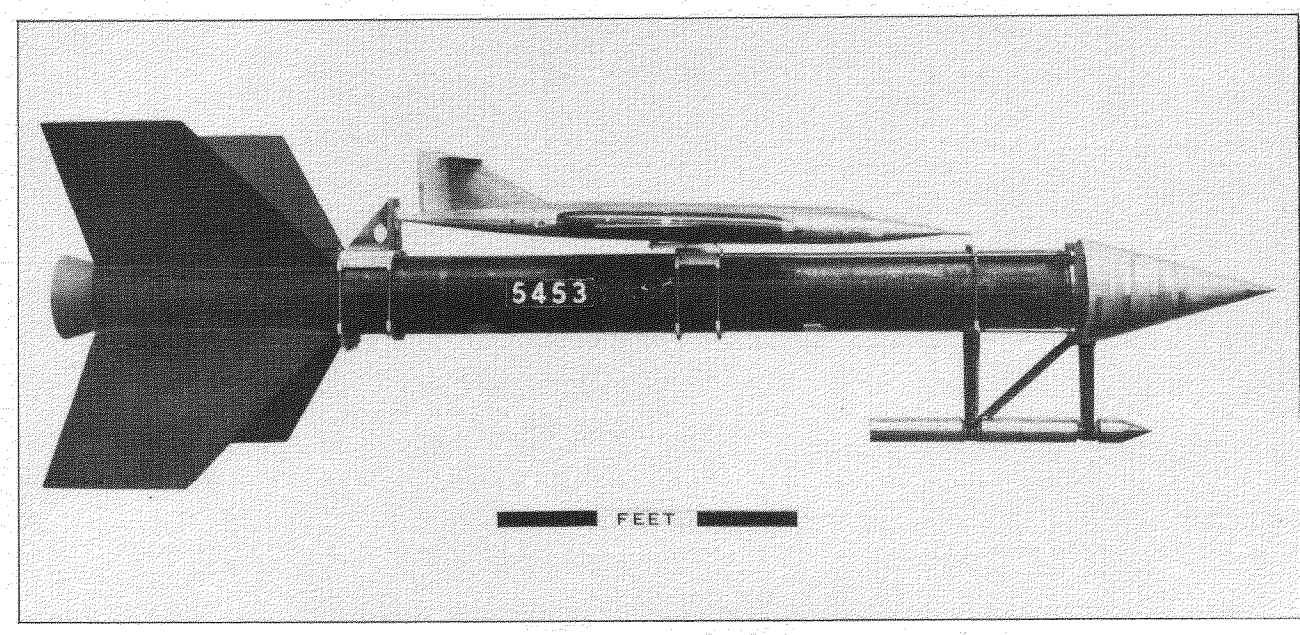

e. MODEL 3 AND BOOST ASSEMBLY

FIG.4d & e. PHOTOGRAPHS OF MODELS

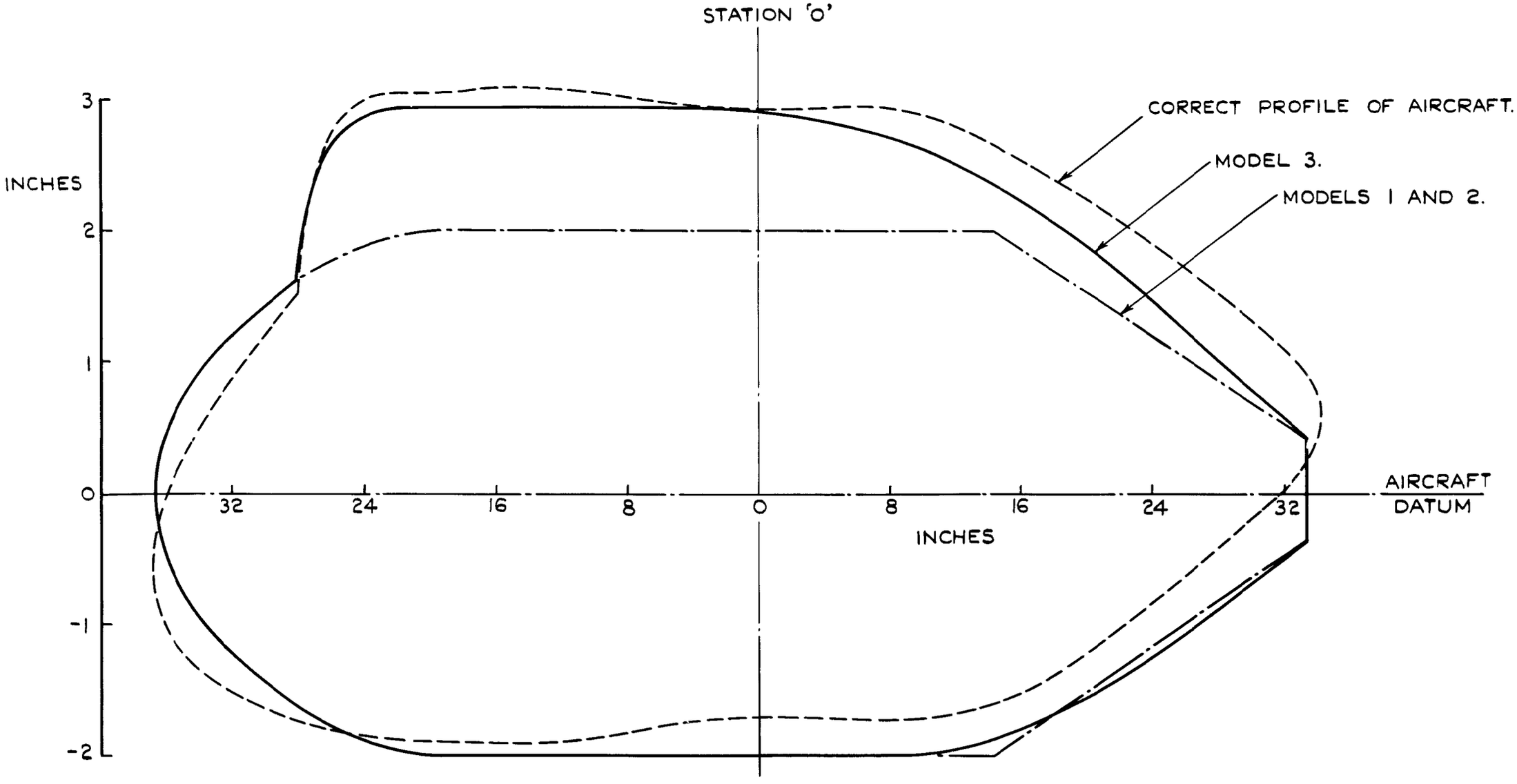

FIG. 5. BODY PROFILES.

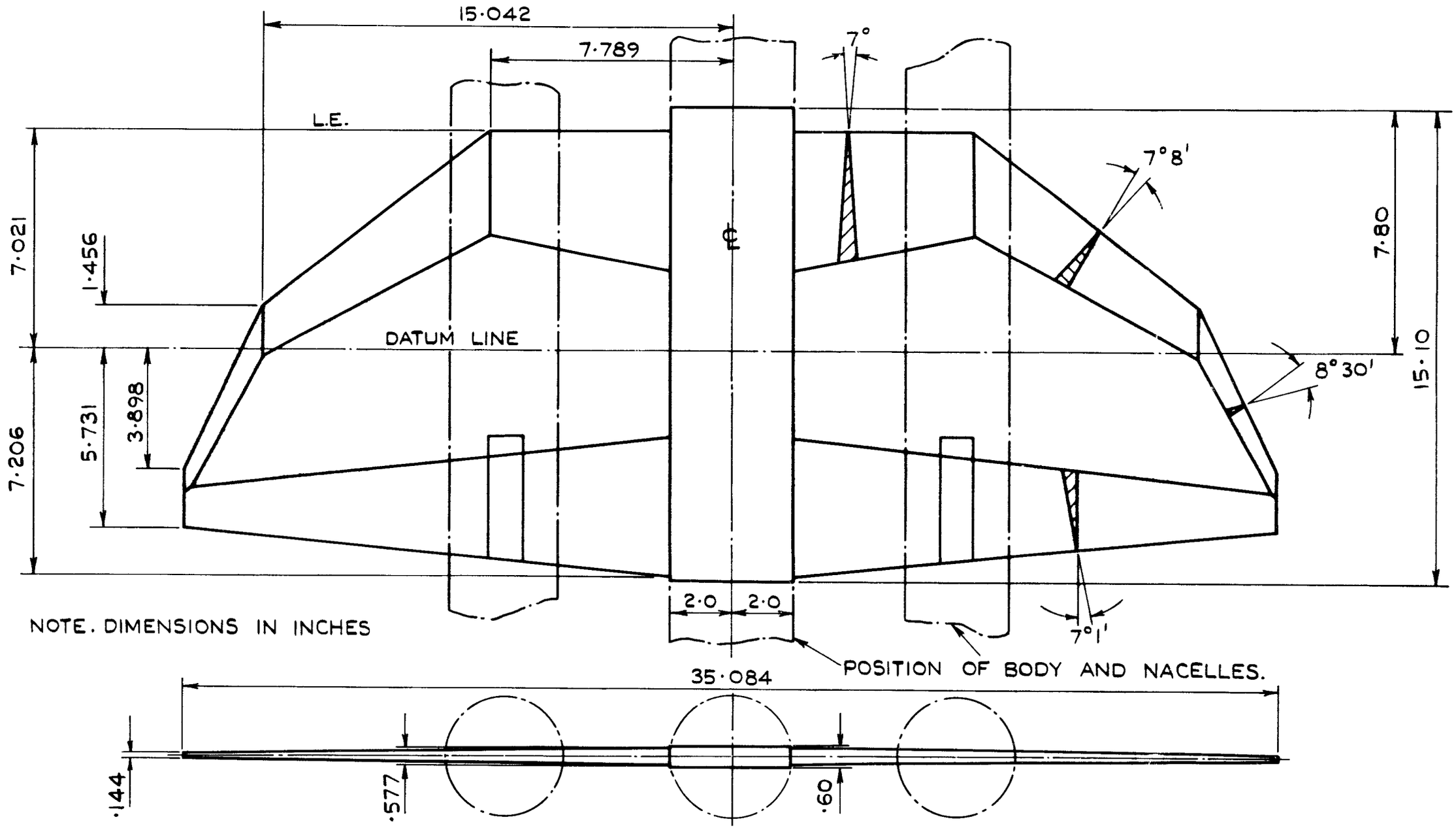

FIG. 6. WING DETAILS.

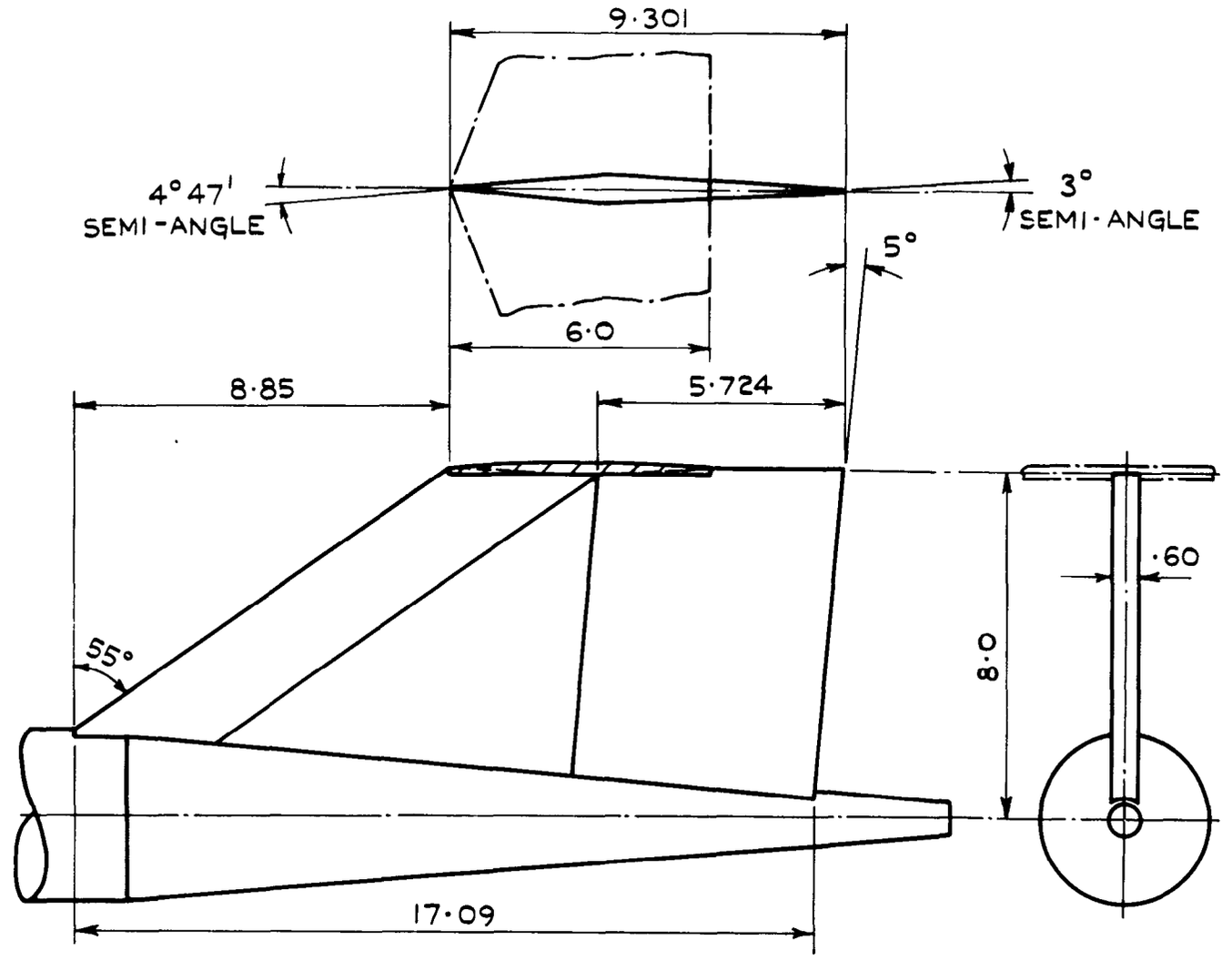

(a) MODELS 1 & 2.

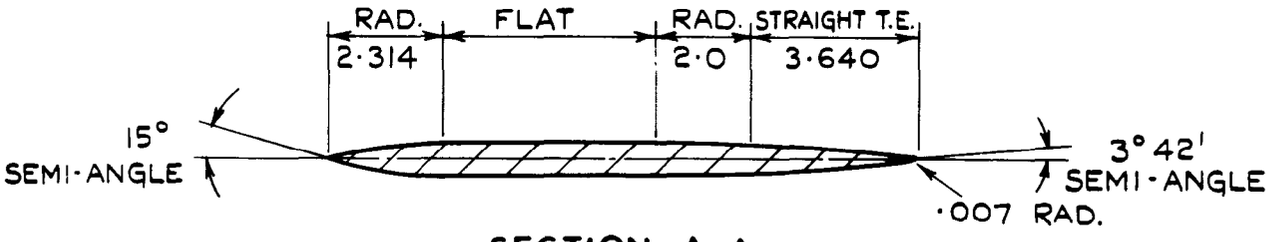

SECTION A-A

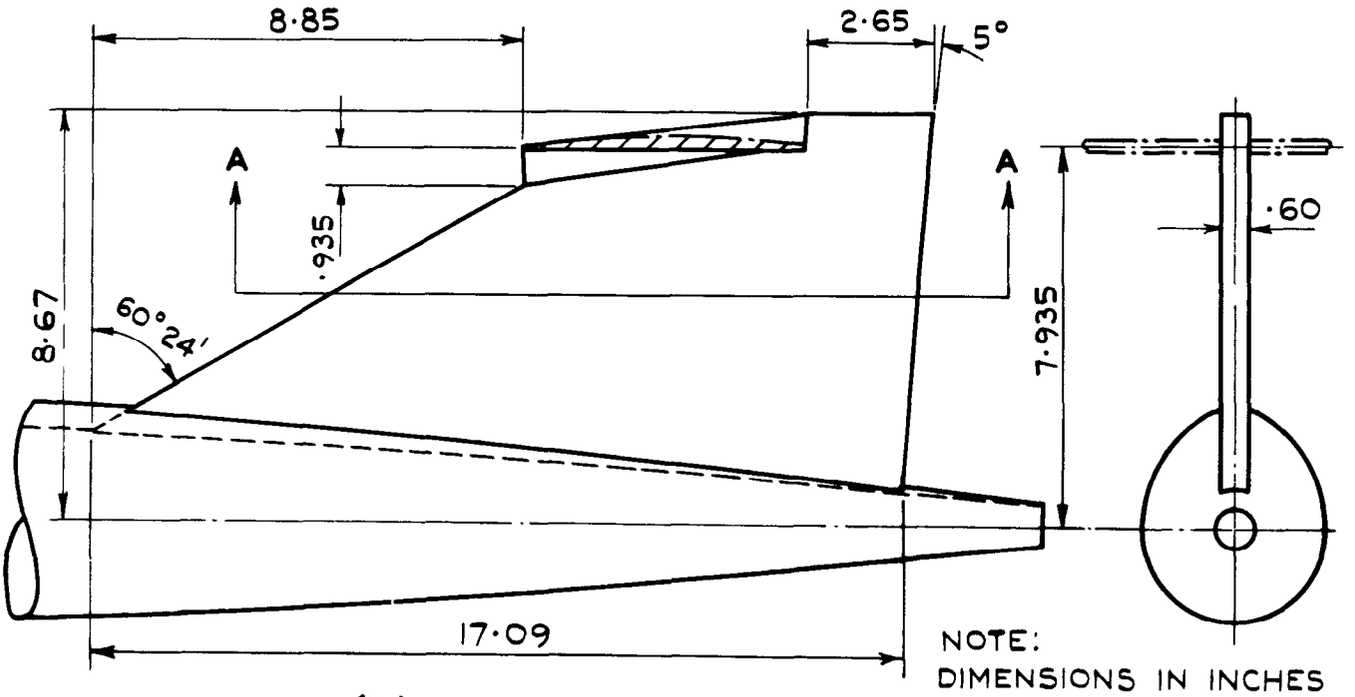

(b) MODEL 3.

FIG. 7. FIN DETAILS.

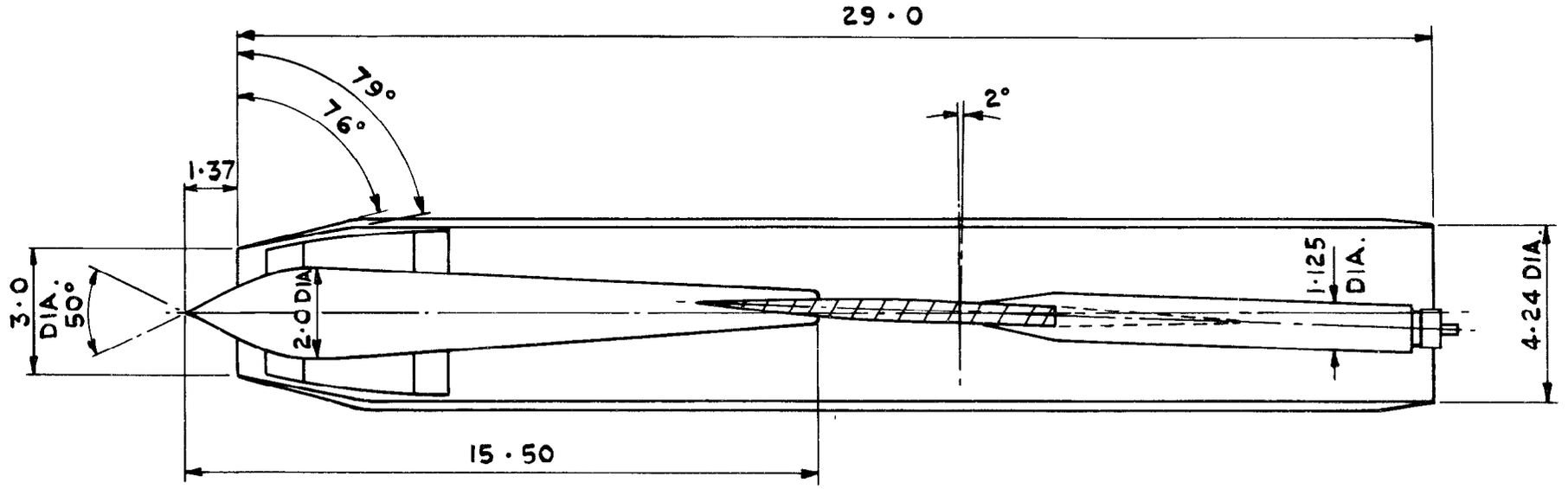

(a) MODELS 1 & 2

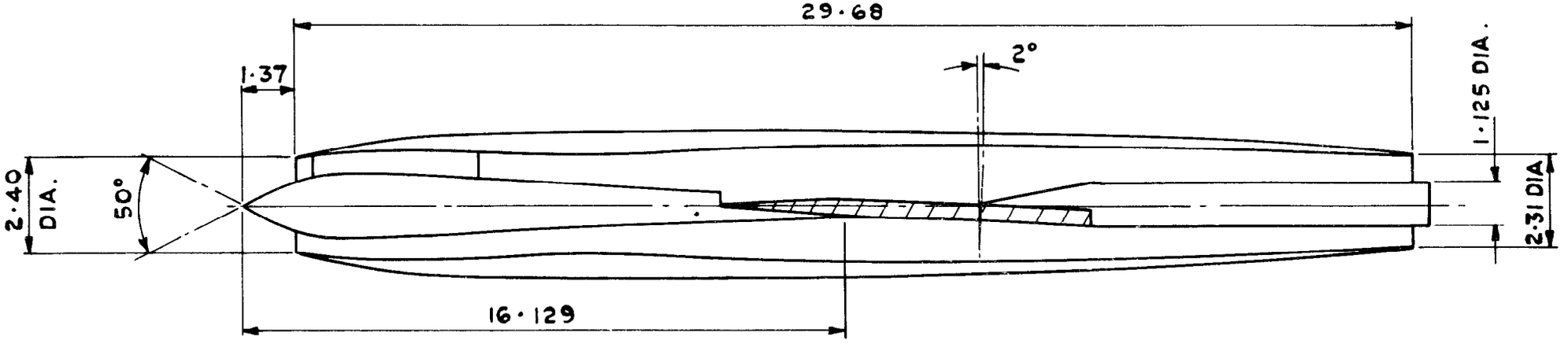

(b) MODEL 3

NOTE - DIMENSIONS IN INCHES

FIG. 8 NACELLE DETAILS.

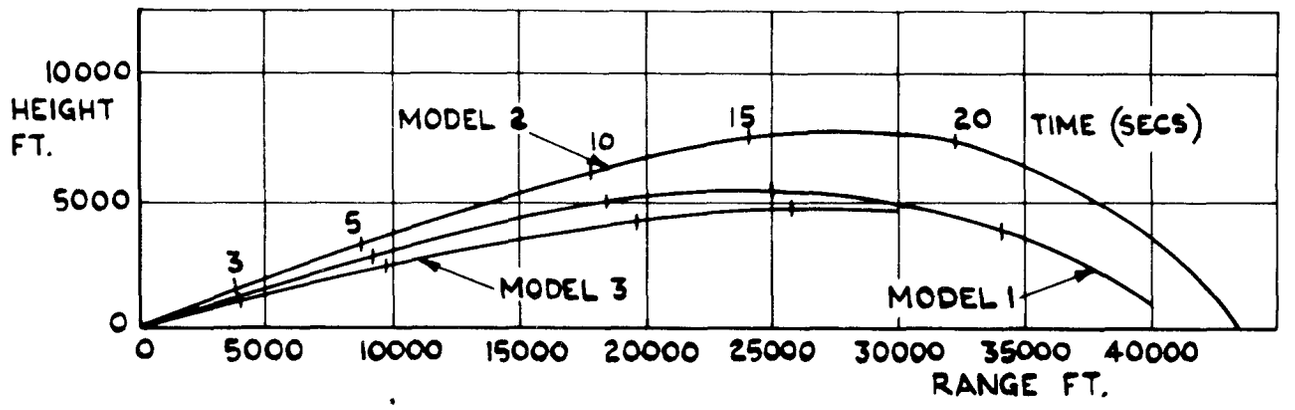

FIG. 9 TRAJECTORIES (MODELS 1, 2, 3.)

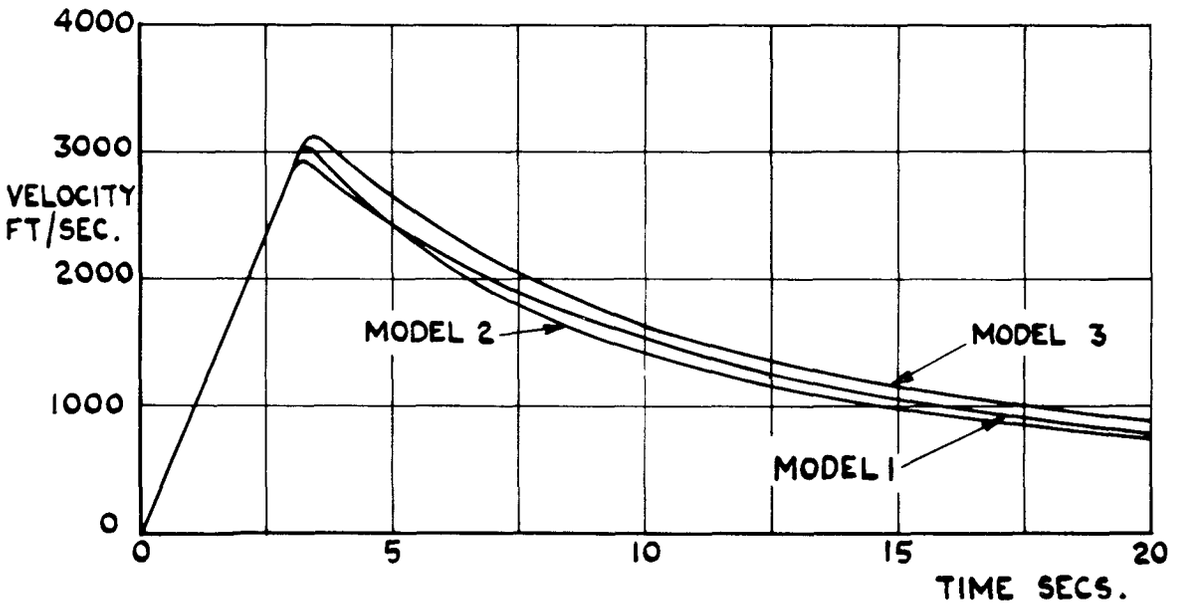

FIG. 10 VELOCITY (MODELS 1, 2, 3.)

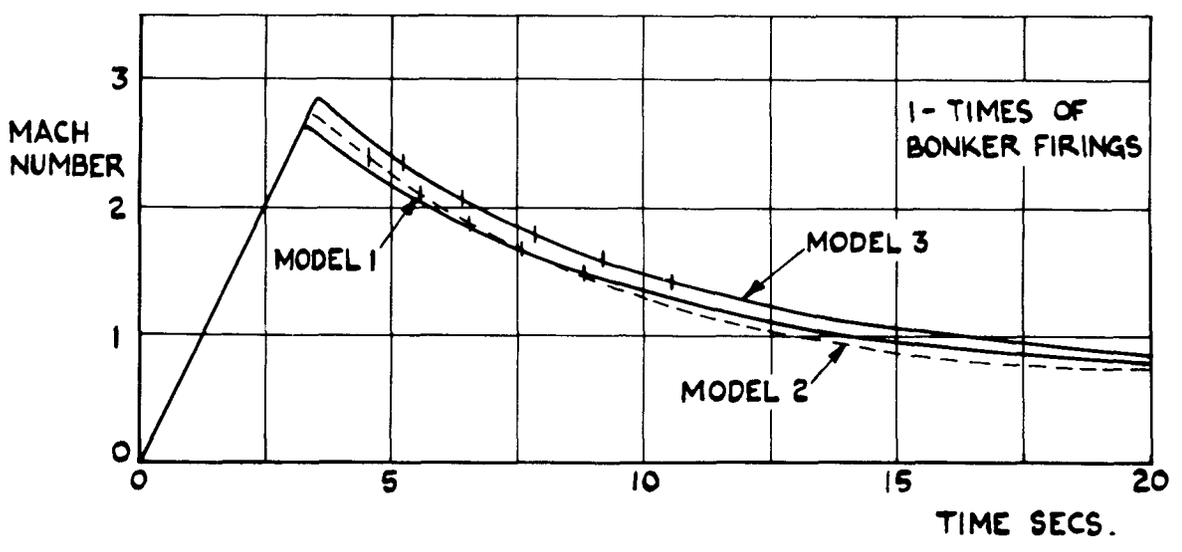

FIG. 11 MACH NUMBER (MODELS 1, 2, 3.)

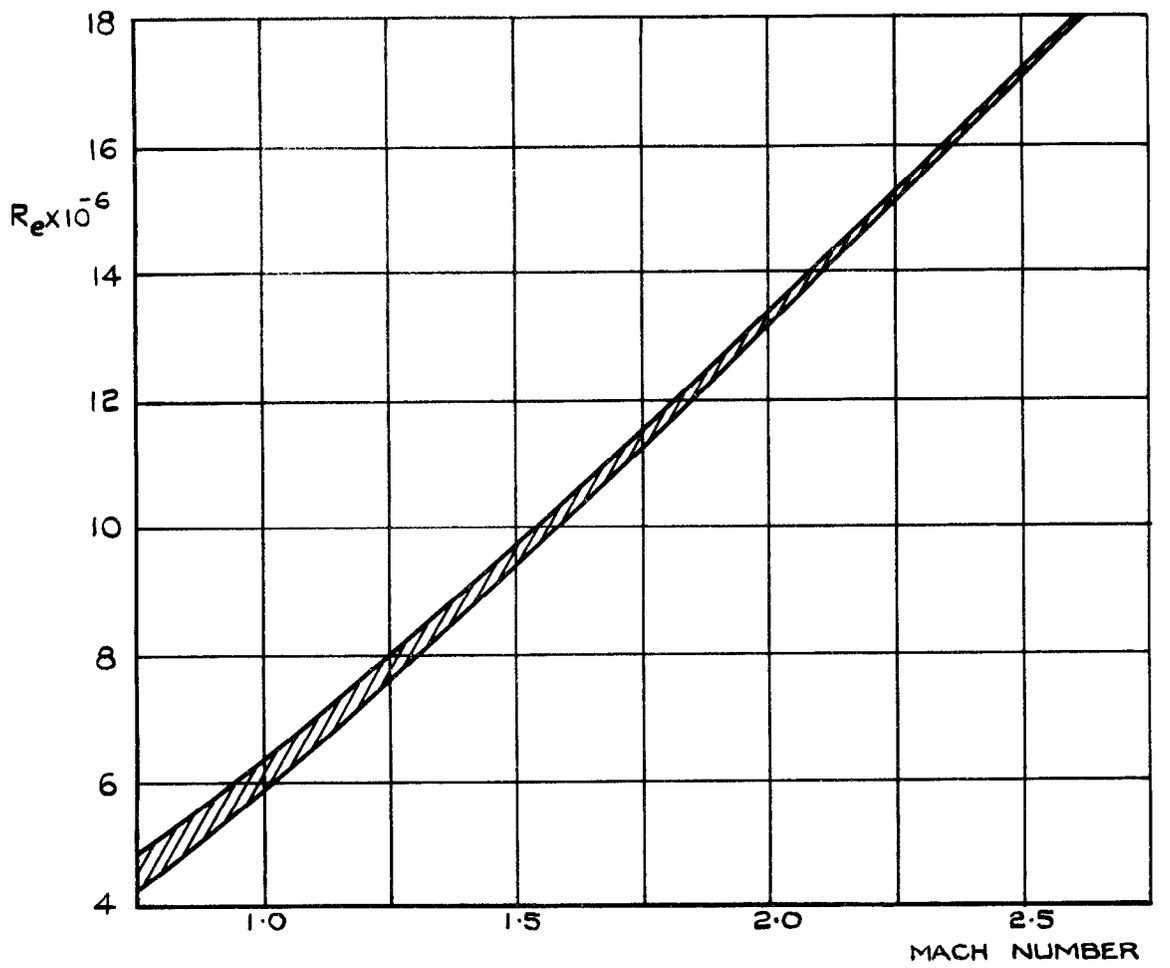

FIG. 12. RANGE OF REYNOLD'S NUMBER (MODELS 1,2 & 3.)

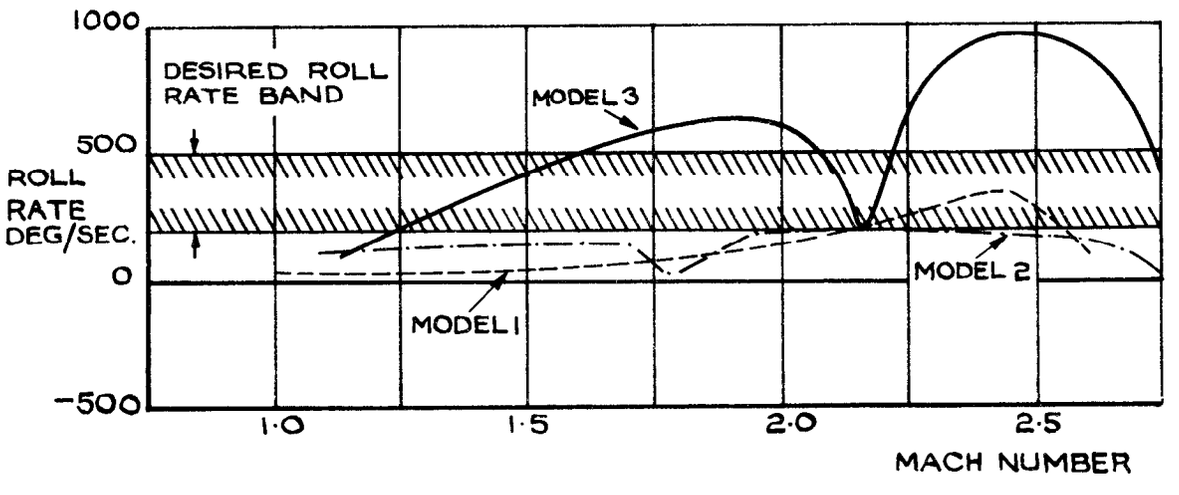

FIG. 13. SUPERIMPOSED STEADY RATE OF ROLL.

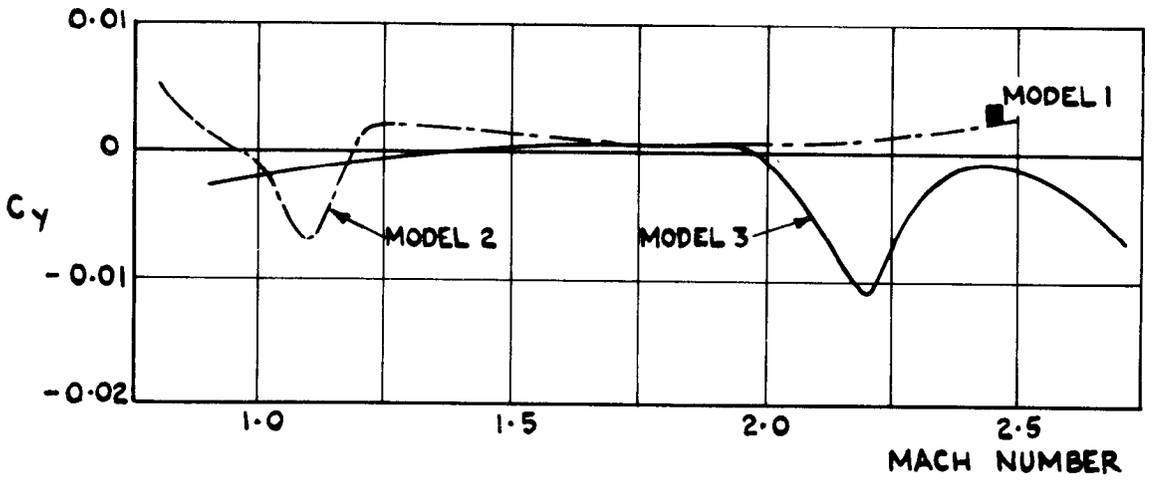

FIG.14 MEAN SIDE-FORCE COEFFICIENT.

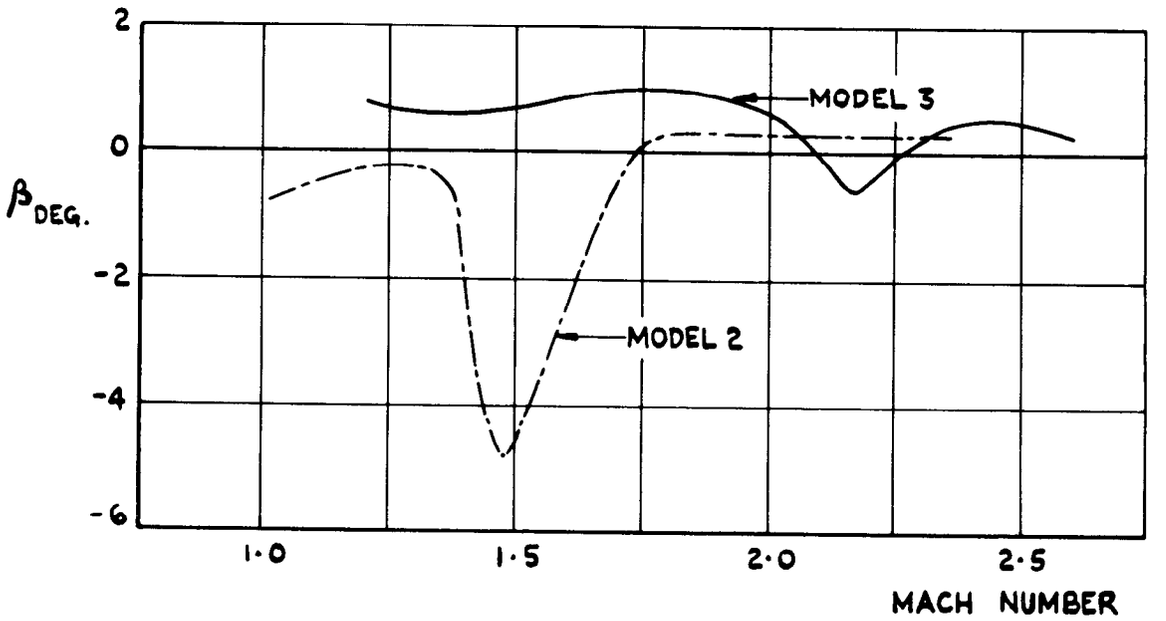

FIG.15 MEAN SIDESLIP ANGLE.

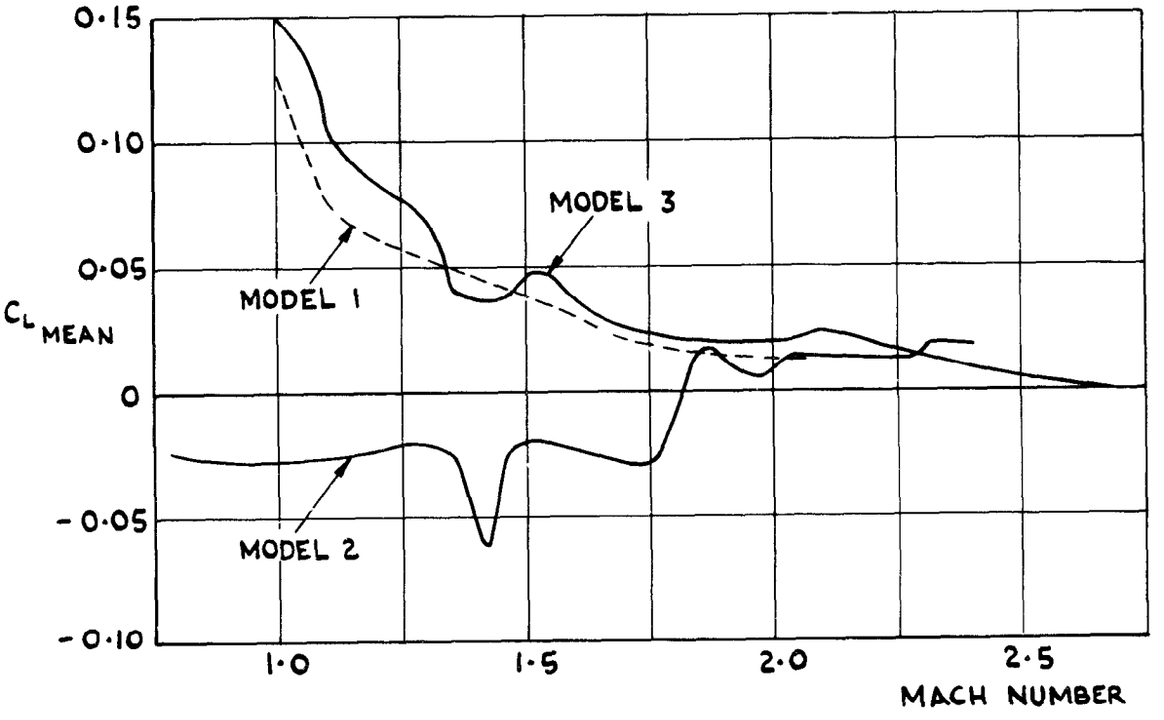

FIG.16 MEAN LIFT COEFFIENT (MODELS 1,2,3)

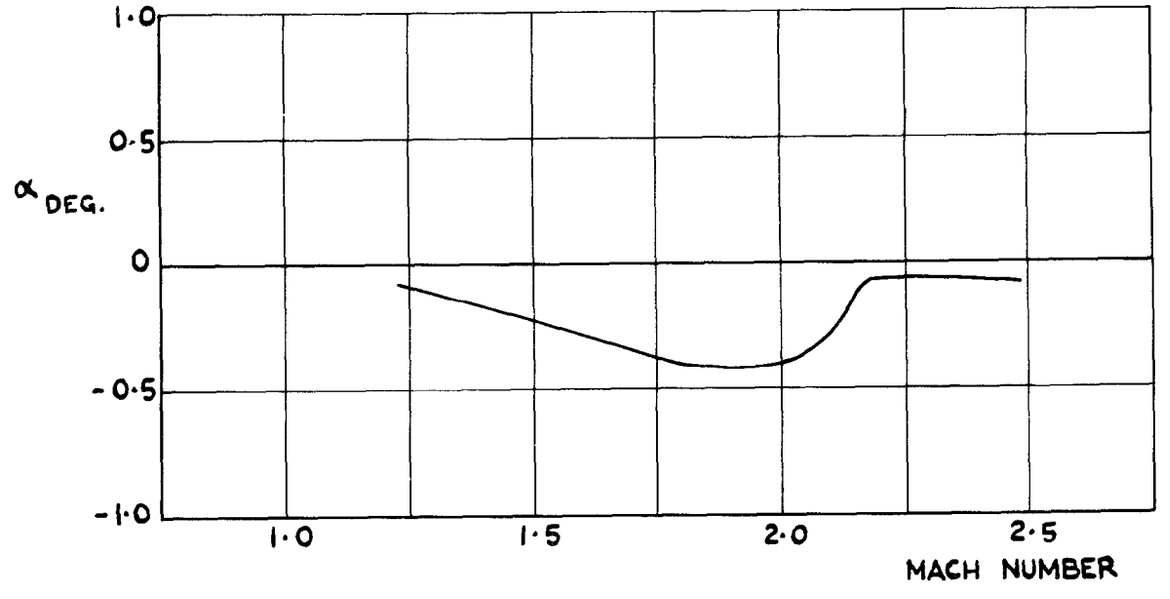

FIG. 17 MEAN INCIDENCE (RELATIVE TO BODY AXIS) (MODEL 3).

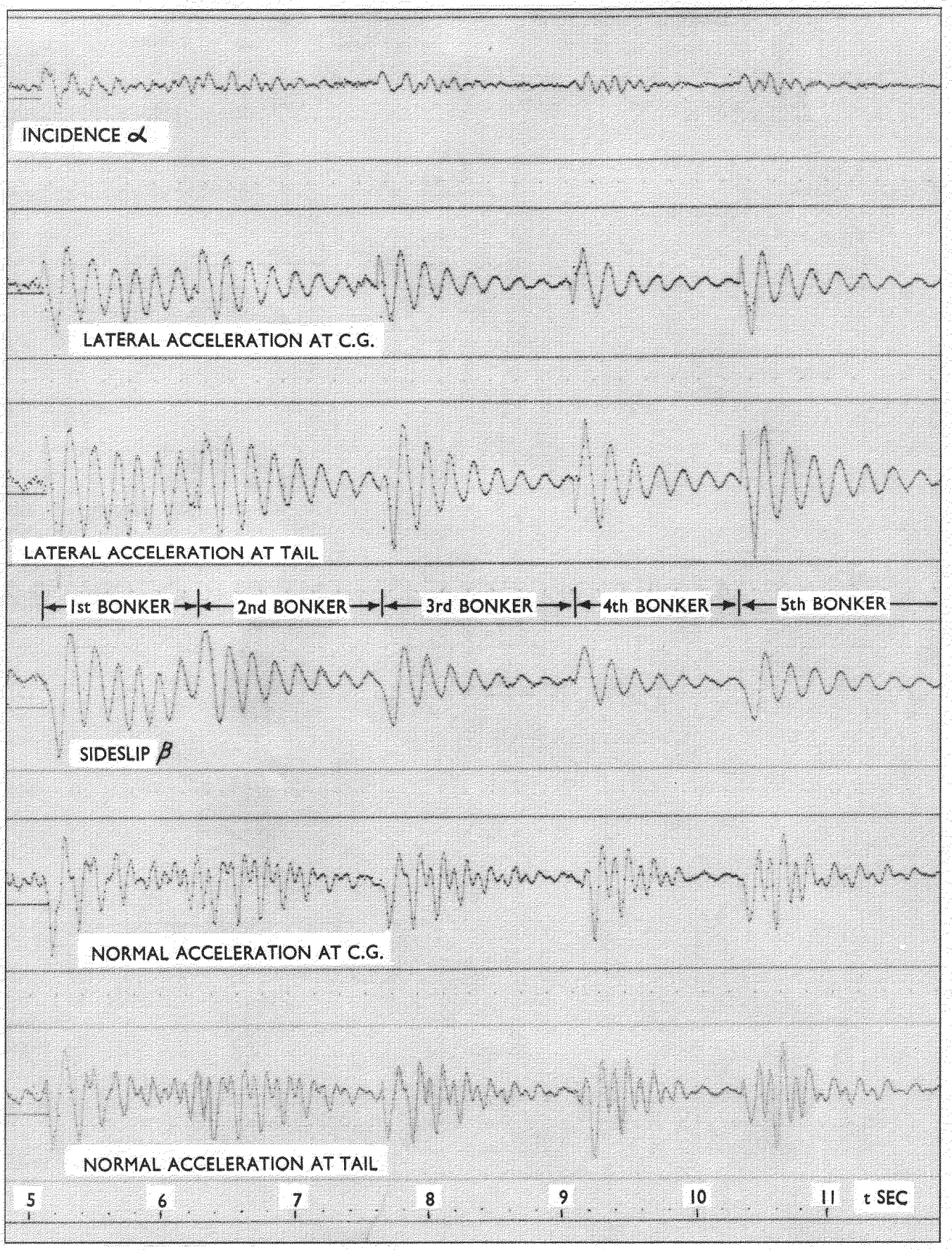

FIG.18. SAMPLE OF TELEMETRY RECORD (MODEL 3)

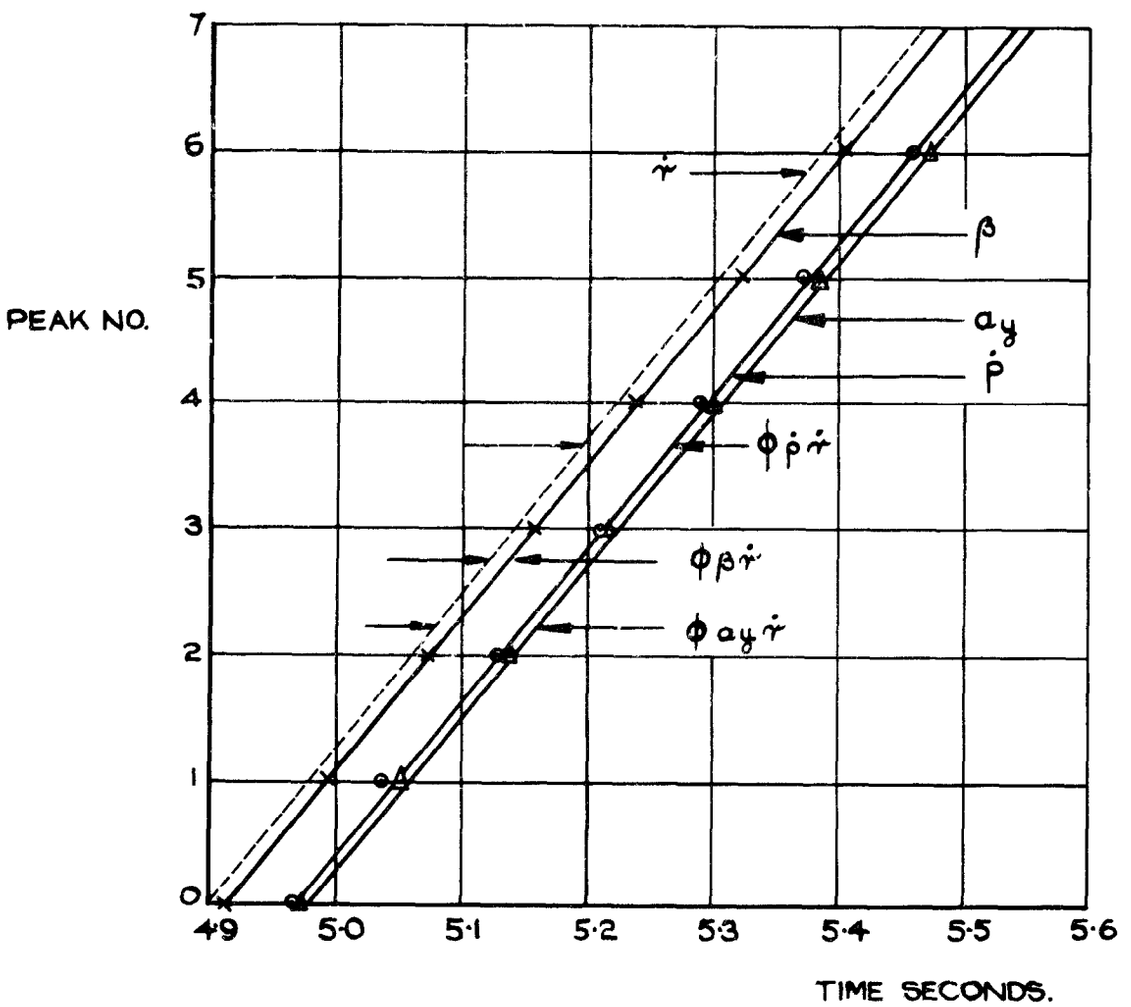

FIG. 19. SAMPLE OF DATA FOR DETERMINING FREQUENCY AND PHASE RELATIONSHIPS OF THE DUTCH ROLL OSCILLATION.
(MODEL 2. OSCILLATION 1.)

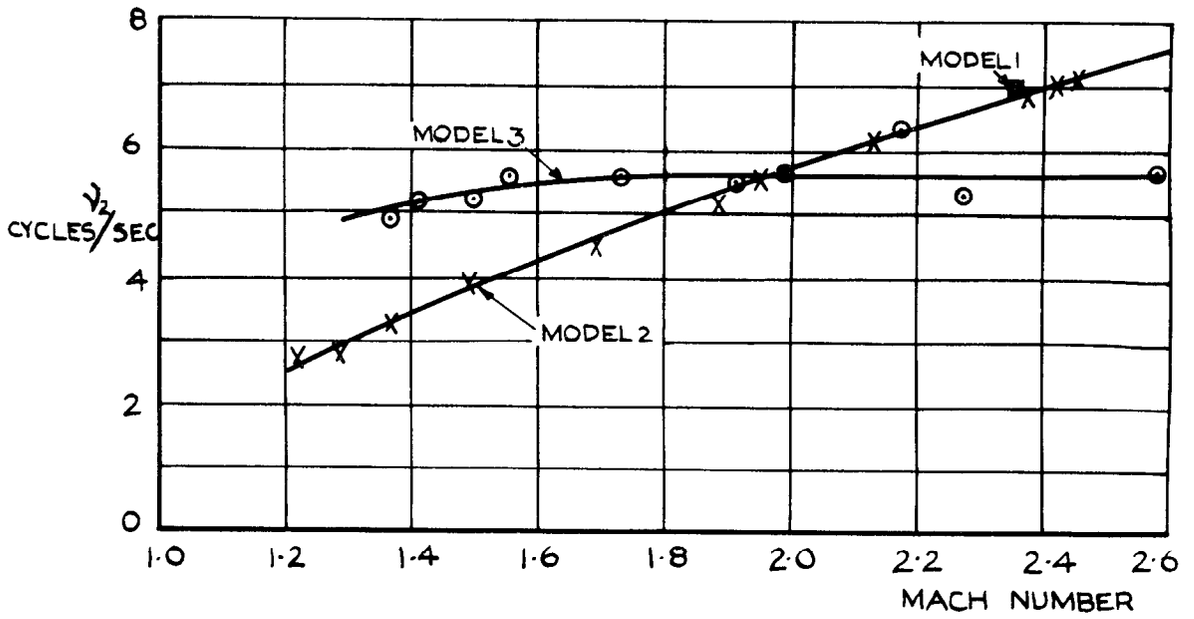

FIG. 20. NATURAL FREQUENCY OF DUTCH-ROLL OSCILLATION.

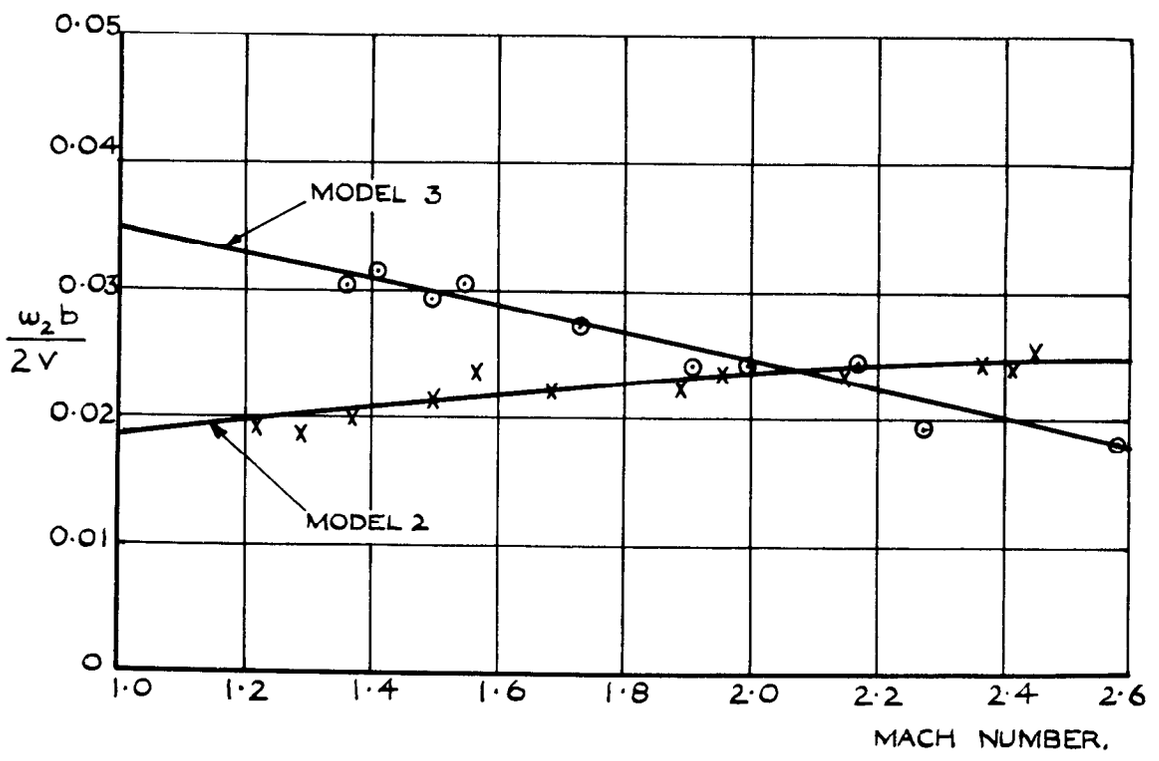

FIG. 21. NON-DIMENSIONAL FREQUENCY PARAMETER OF DUTCH-ROLL OSCILLATION.

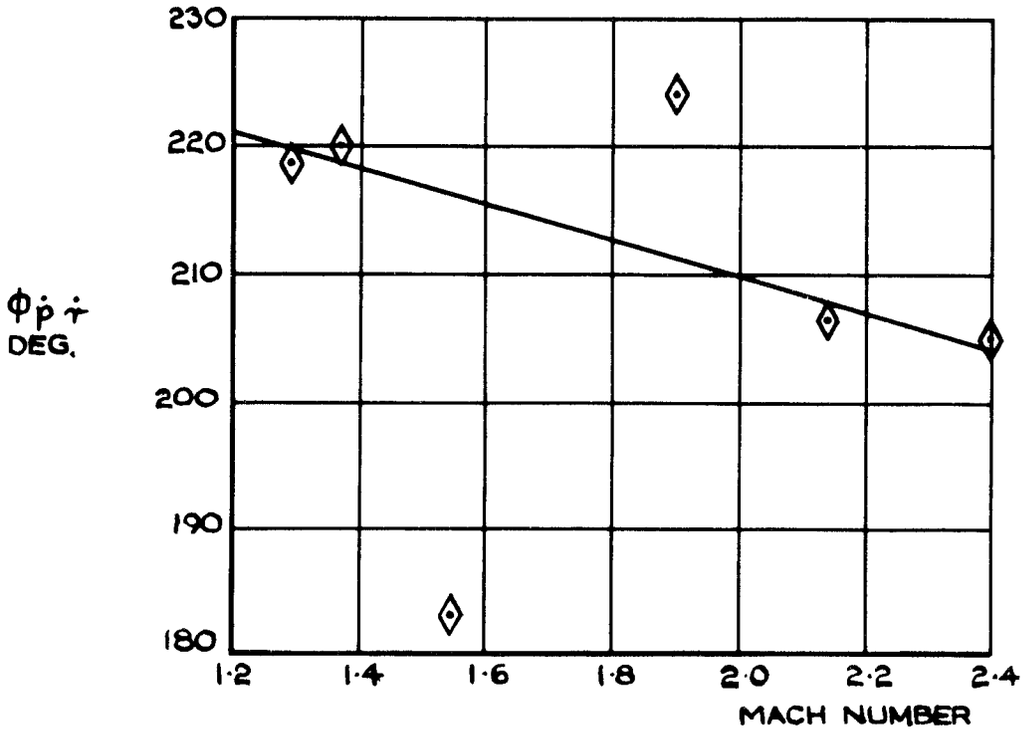

(a) ROLL–YAW PHASE ANGLE.

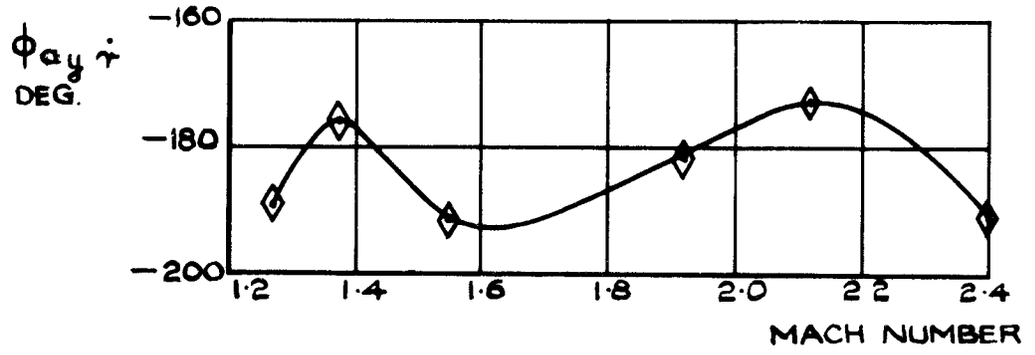

(b) LATERAL ACCELERATION–YAW PHASE ANGLE.

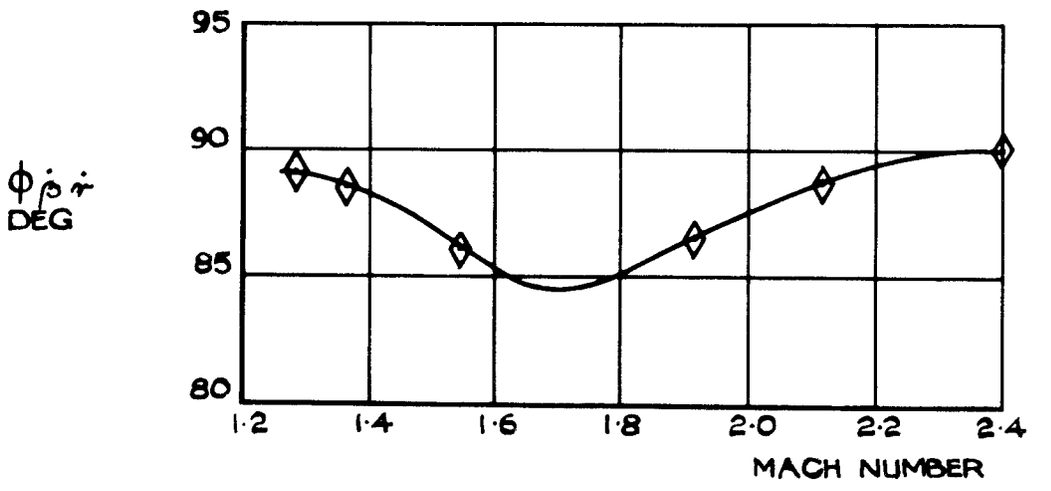

(c) SIDESLIP–YAW PHASE ANGLE.

FIG. 22. PHASE RELATIONSHIPS OF DUTCH-ROLL OSCILLATION (MODEL 2.)

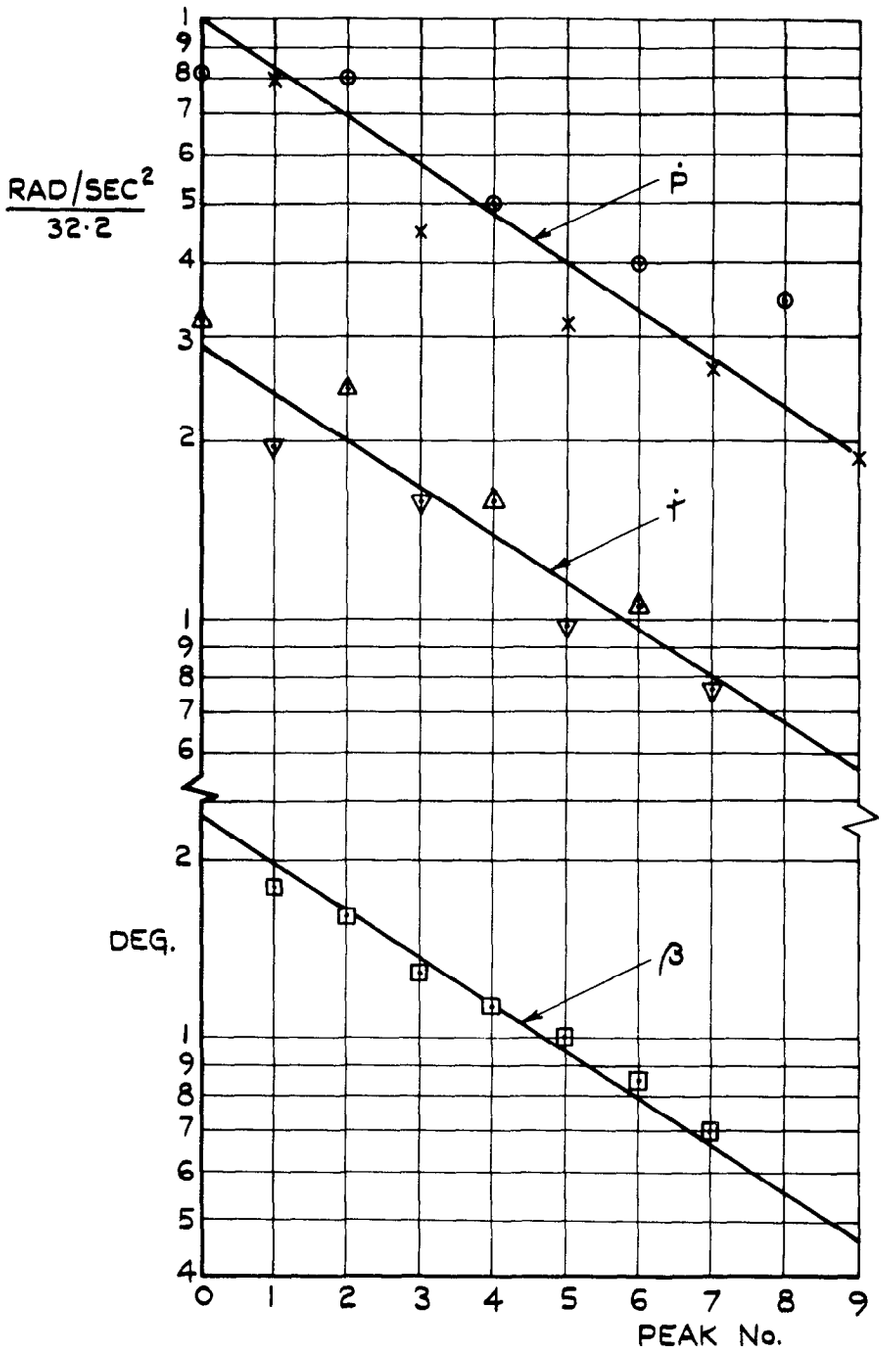

FIG. 23. SAMPLE OF DATA FOR DETERMINING DAMPING OF THE DUTCH - ROLL OSCILLATION.
(MODEL 2, OSCILLATION 1)

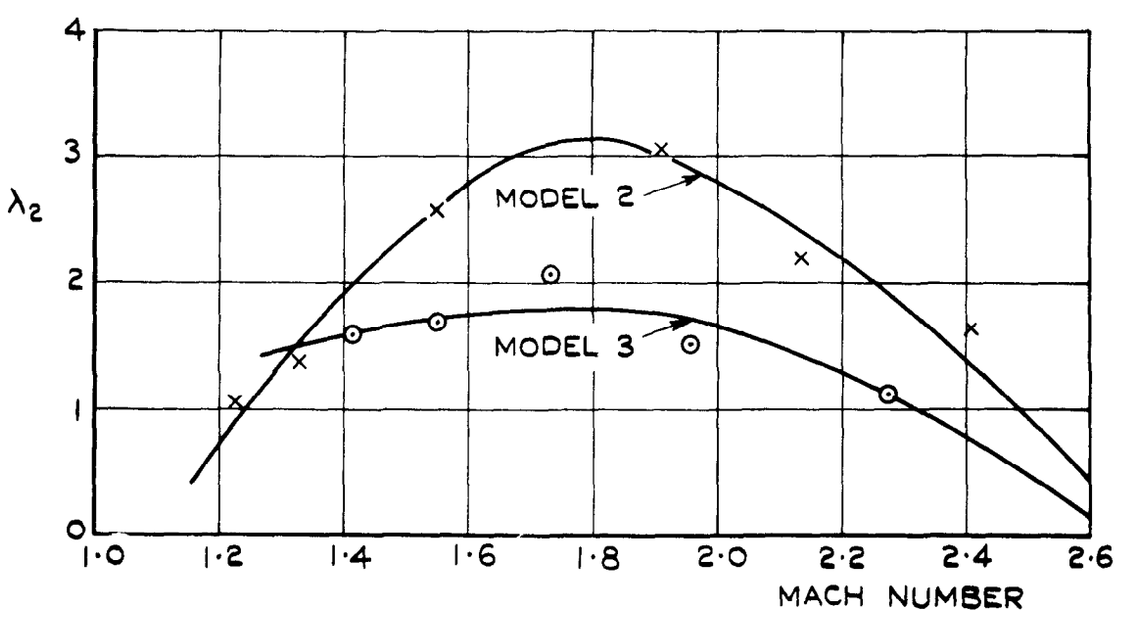

FIG. 24. DAMPING OF DUTCH - ROLL OSCILLATION.

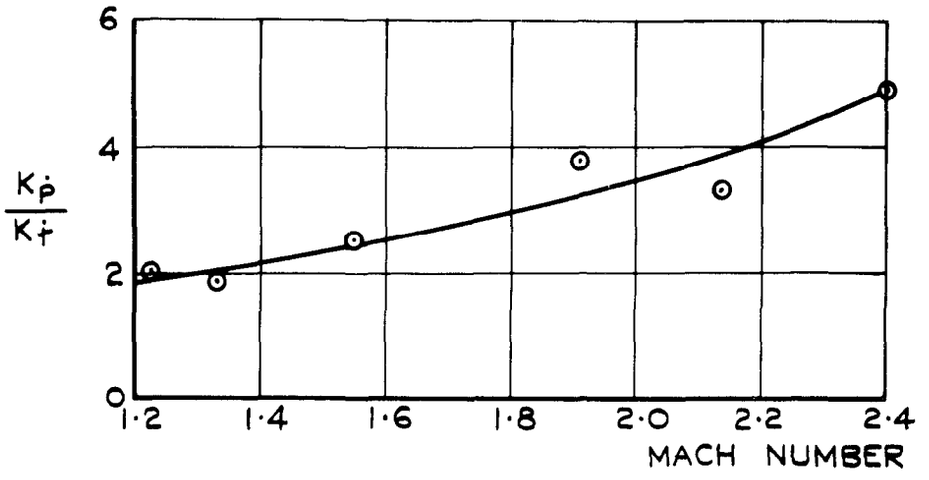

(a) ROLL - YAW RATIO.

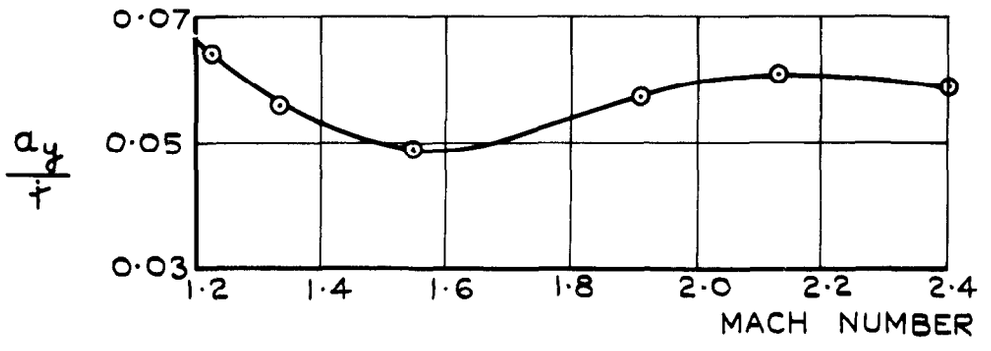

(b) LATERAL ACCELERATION - YAW RATIO.

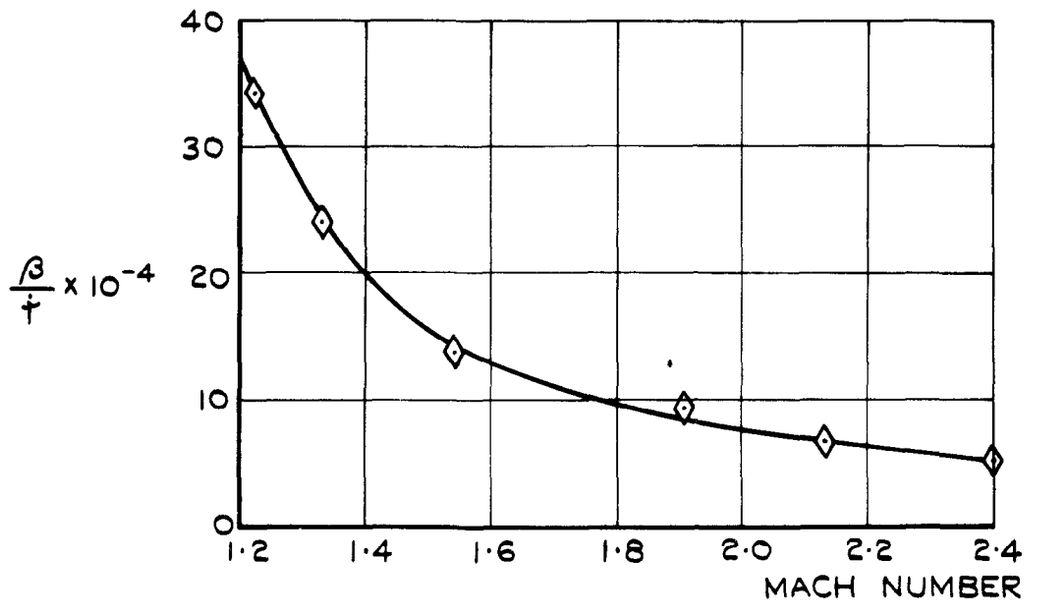

(c) SIDESLIP - YAW RATIO.

FIG. 25. AMPLITUDE RATIOS OF DUTCH - ROLL OSCILLATION (MODEL 2.)

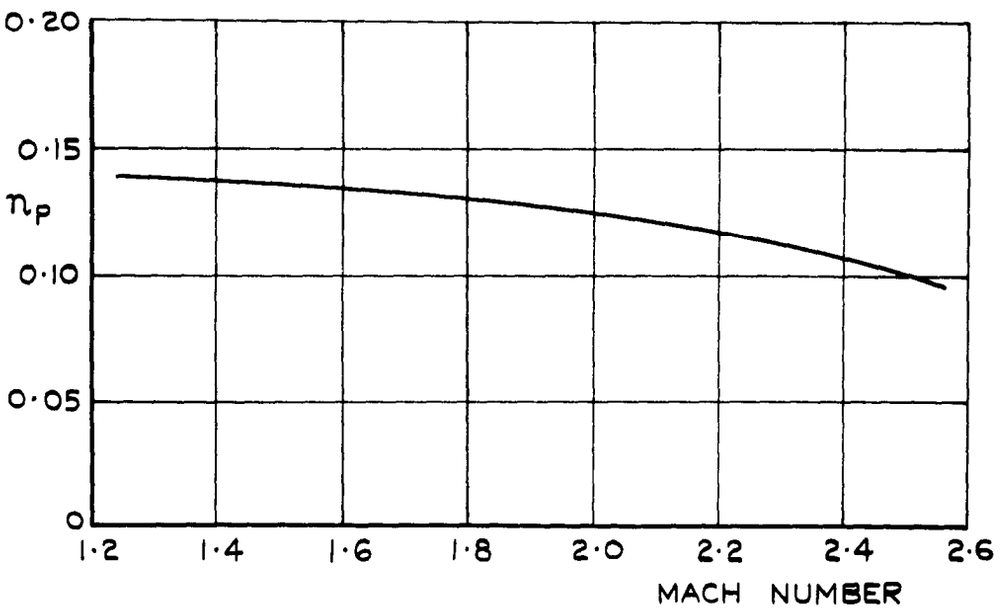

FIG. 26. ESTIMATED VALUES OF n_p.

(LINEARISED THEORY - FIN EFFECT ONLY)

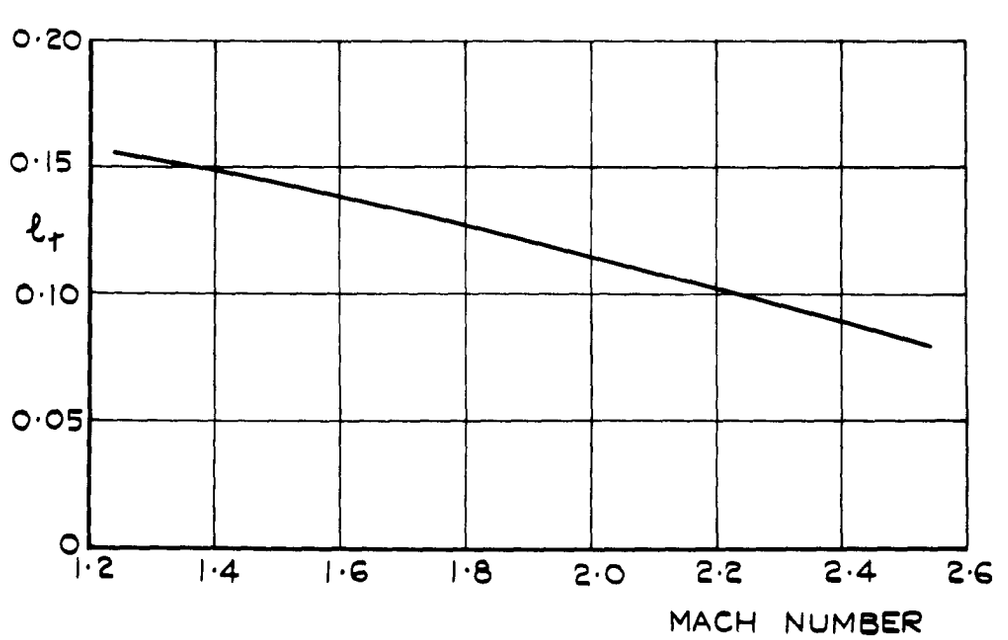

FIG. 27. ESTIMATED VALUES OF l_f.

(LINEARISED THEORY - FIN EFFECT ONLY)

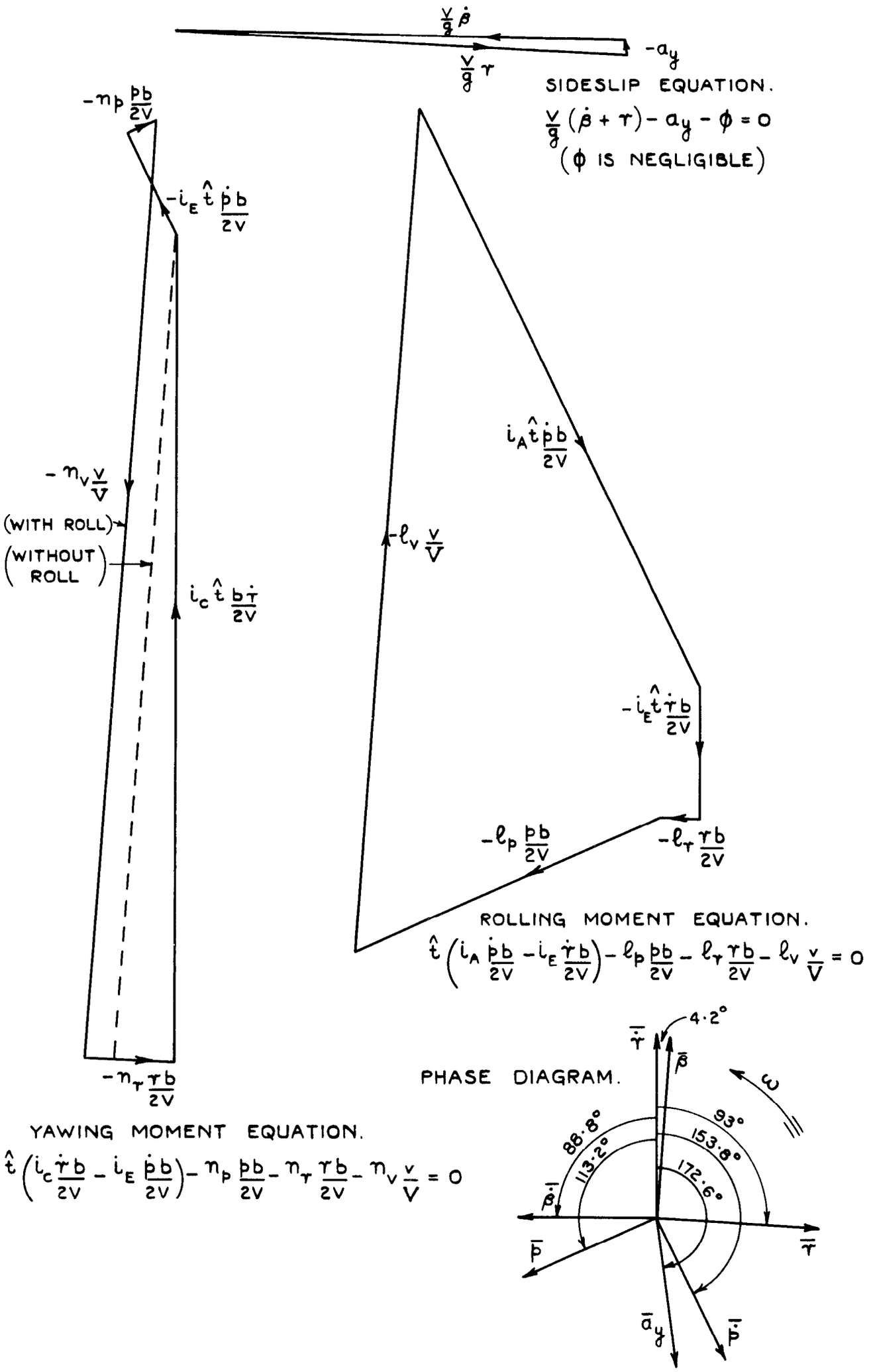

FIG. 28. VECTOR DIAGRAM OF DUTCH-ROLL OSCILLATION.

(MODEL 2, OSCILLATION No. 2)

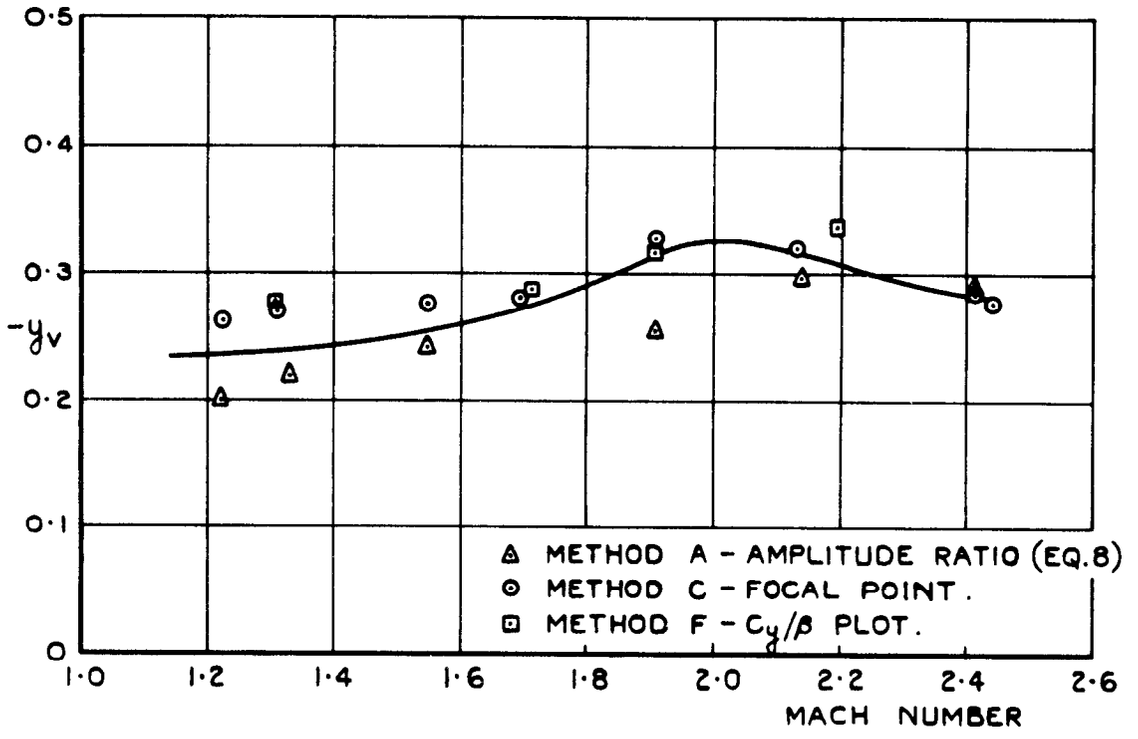

(a) MODEL 2.

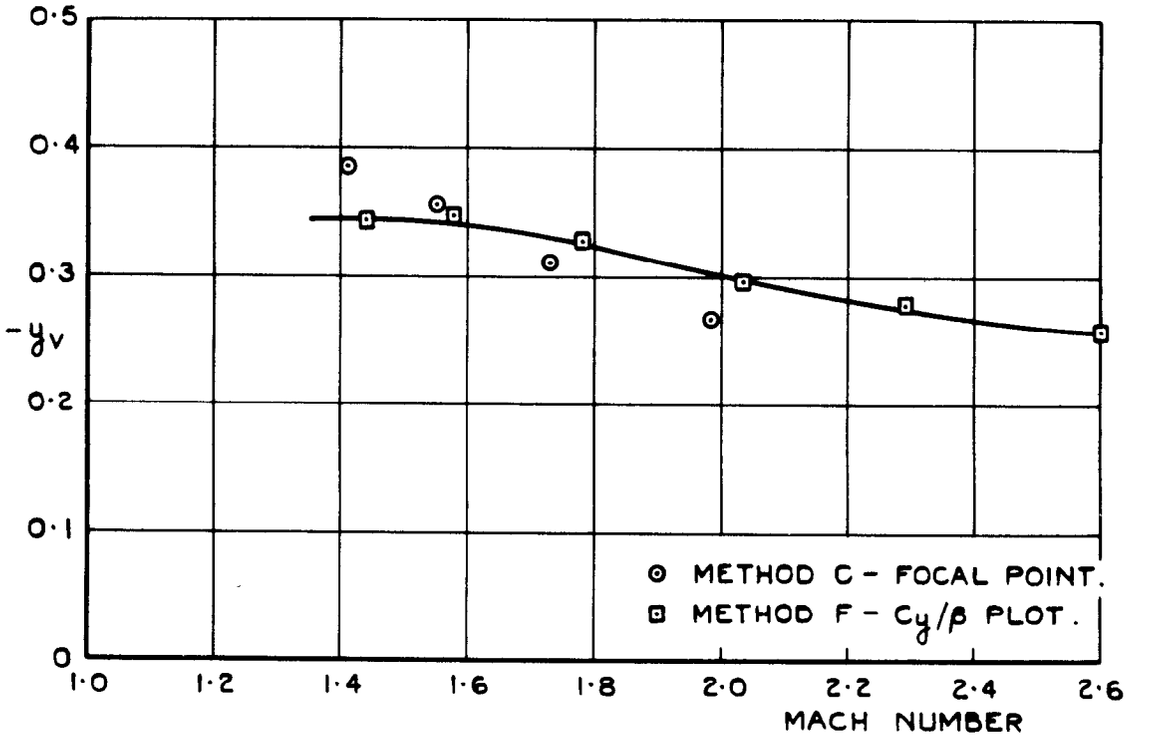

(b) MODEL 3.

FIG. 29. SIDEFORCE DERIVATIVE y_v.

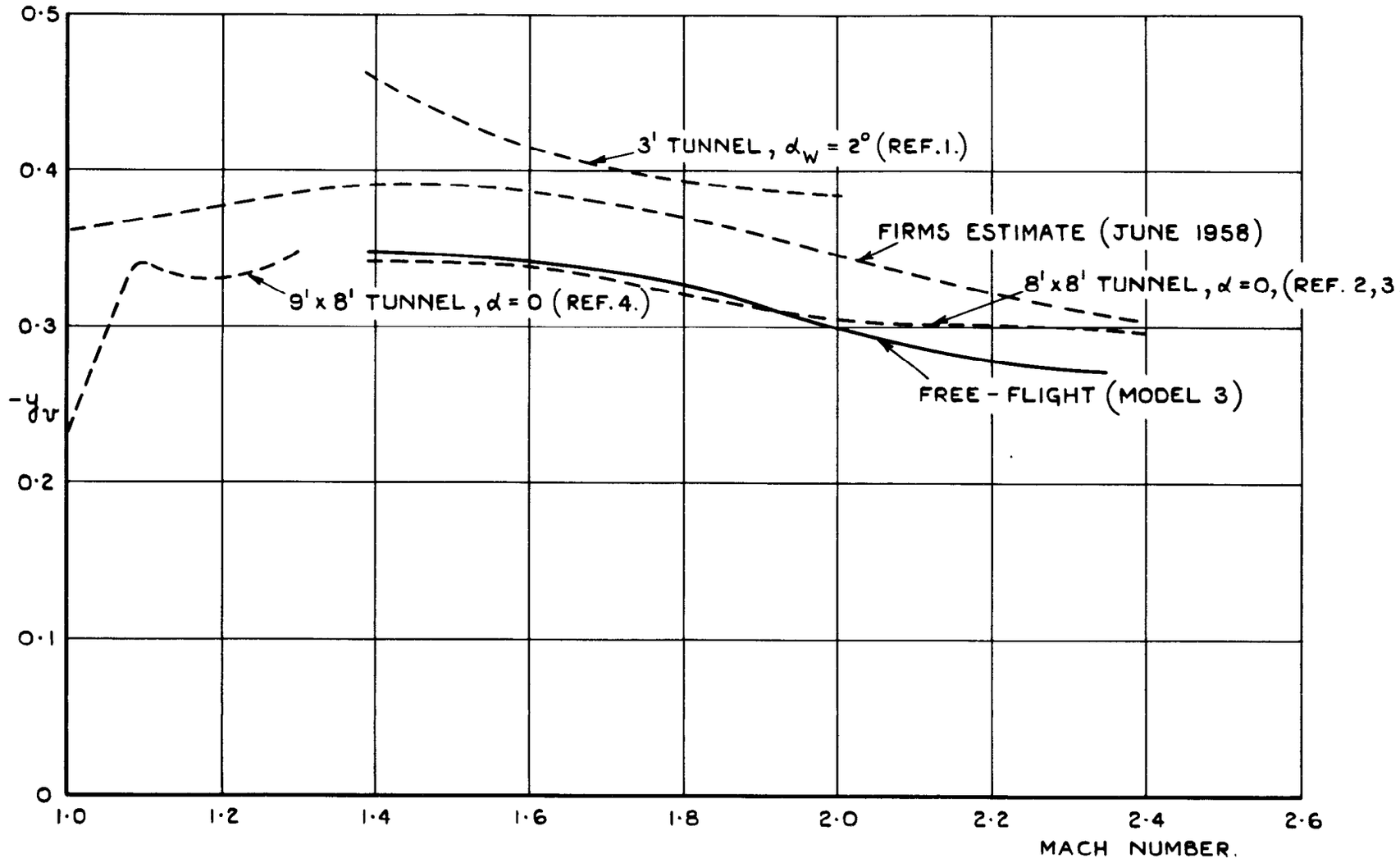

(C) COMPARISON OF VALUES OF SIDEFORCE DERIVATIVE y_v FROM FREE-FLIGHT, WIND-TUNNELS AND ESTIMATES.

FIG. 29. SIDEFORCE DERIVATIVE y_v.

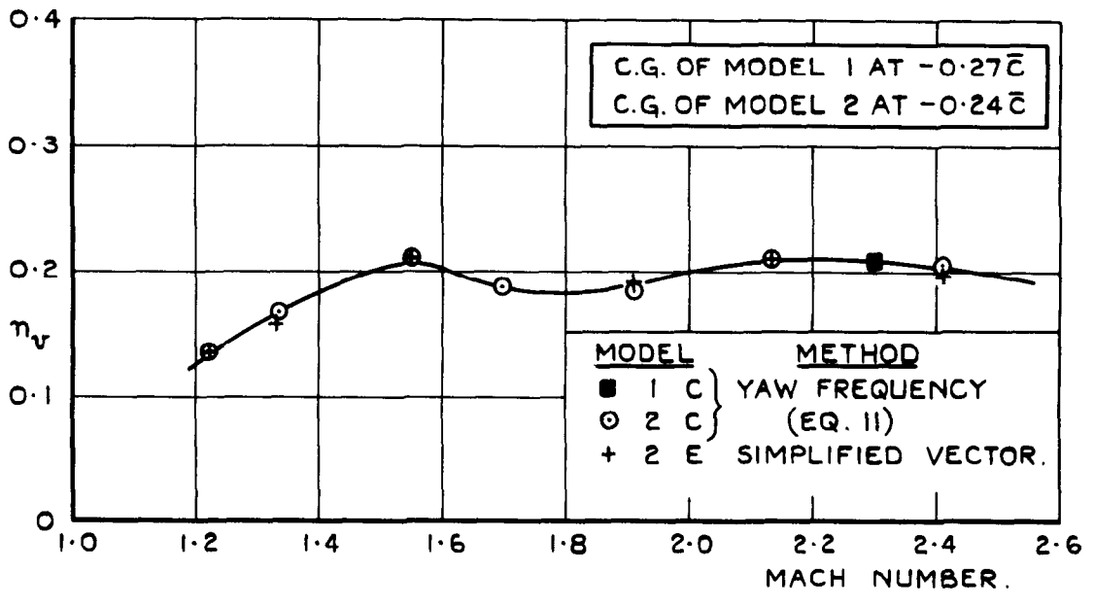

(a) MODELS 1 & 2. TWO-DEGREES-OF-FREEDOM ANALYSIS.

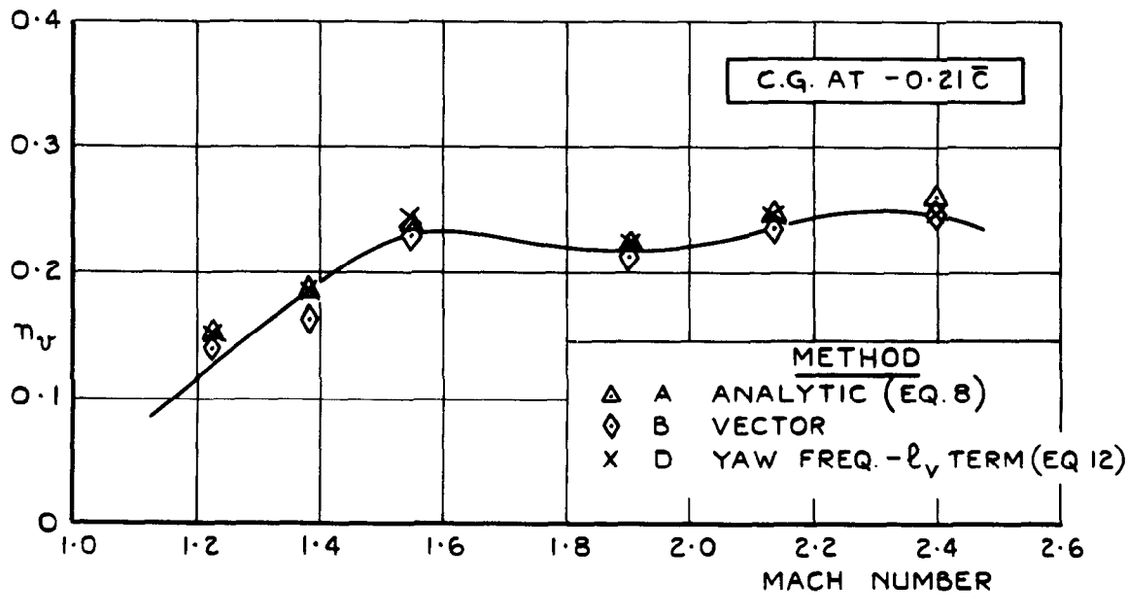

(b) MODEL 2. THREE-DEGREES-OF-FREEDOM ANALYSIS.

FIG. 30. YAWING-MOMENT DERIVATIVE n_v.

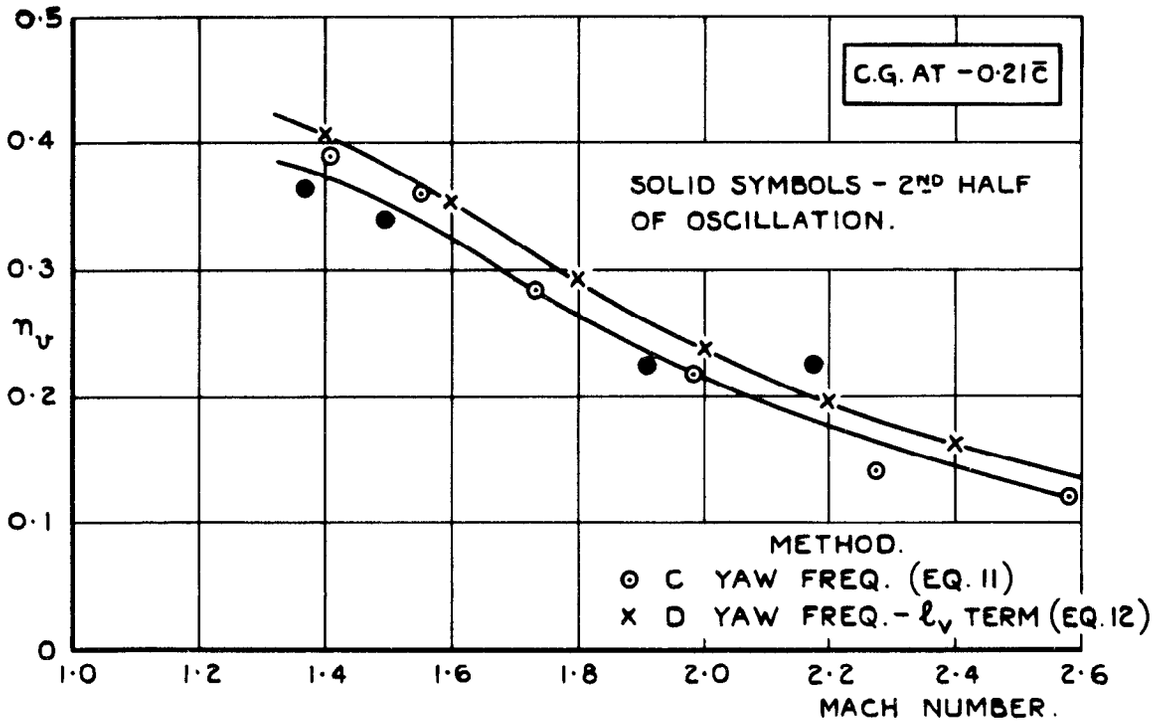

(C) MODEL 3 – TWO-DEGREE-OF-FREEDOM ANALYSIS.

FIG. 30. YAWING-MOMENT DERIVATIVE n_v.

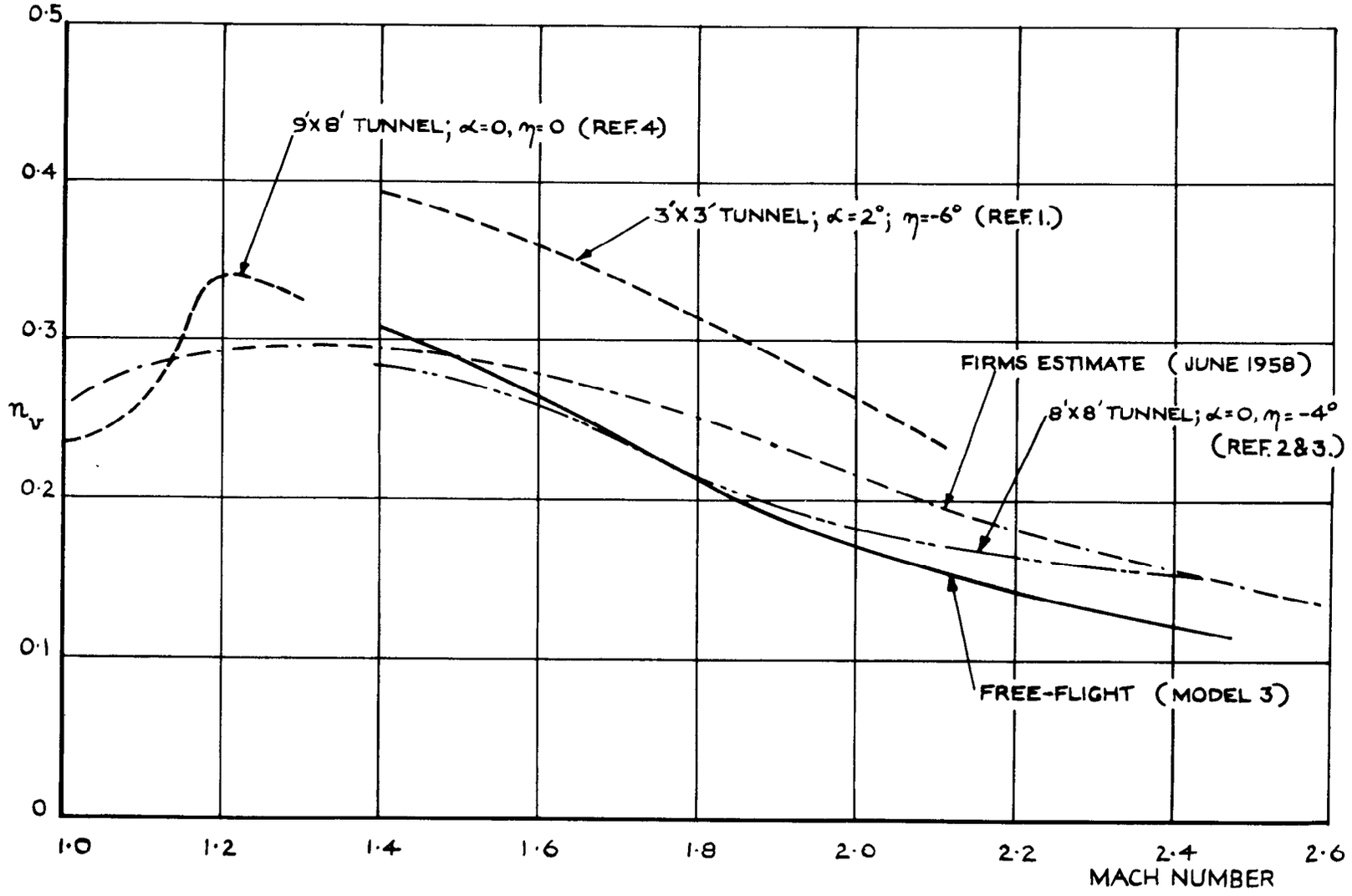

FIG. 31. COMPARISON OF VALUES OF YAWING-MOMENT DERIVATIVE n_v FROM FREE-FLIGHT, WIND-TUNNELS AND ESTIMATES.

(ALL REFERRED TO C.G. AT + 0·18 $\bar{c}$)

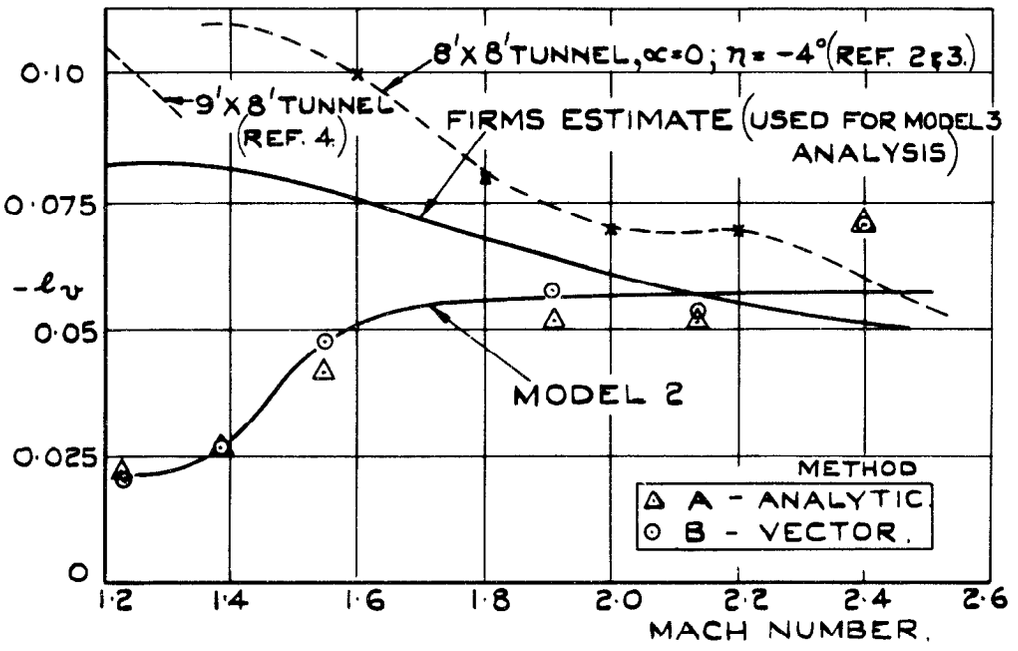

FIG.32. ROLLING MOMENT DUE TO SIDESLIP ℓ_v (MODEL 2)

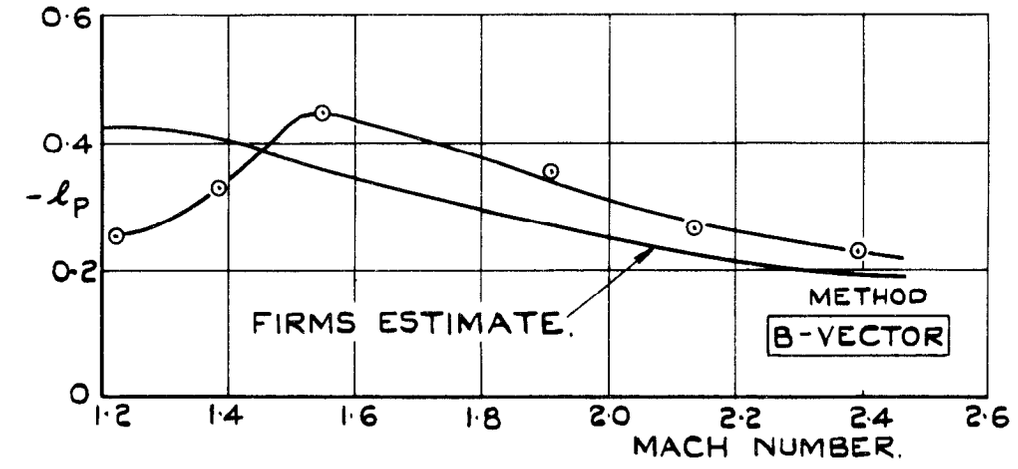

FIG. 33. ROLL-DAMPING DERIVATIVE ℓ_p (MODEL 2)

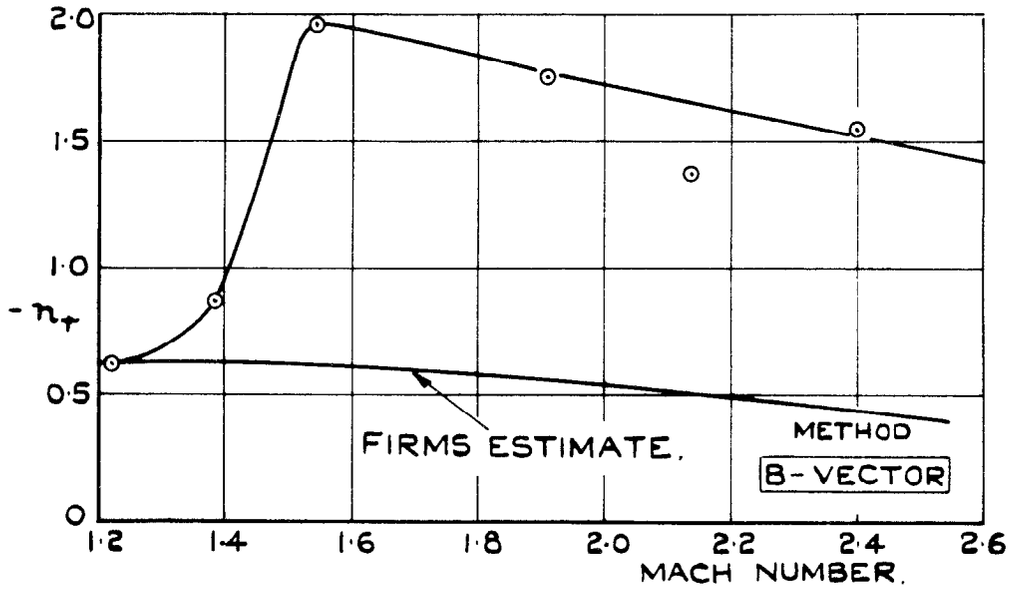

FIG. 34. YAW DAMPING DERIVATIVE n_r (MODEL 2)
(C.G. AT - 0·24 $\bar{c}$.)

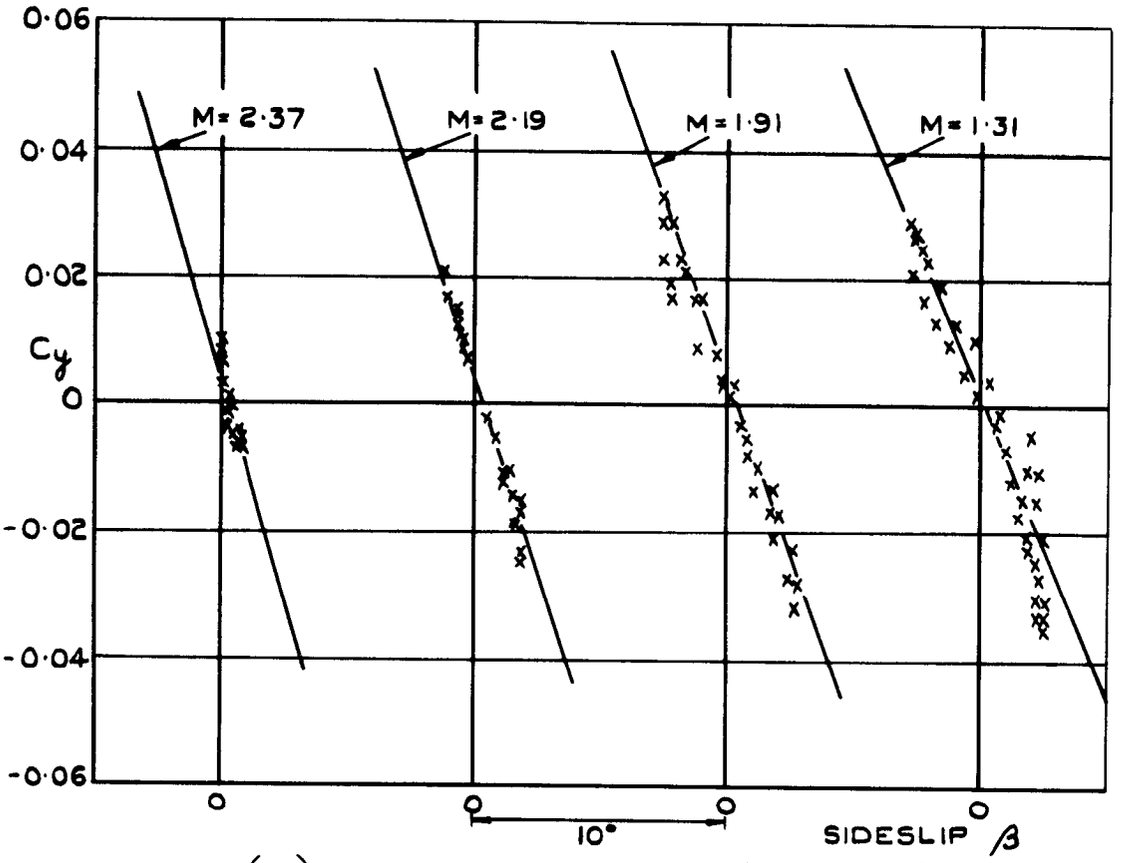

(a) SIDE-FORCE CURVES (MODEL 2)

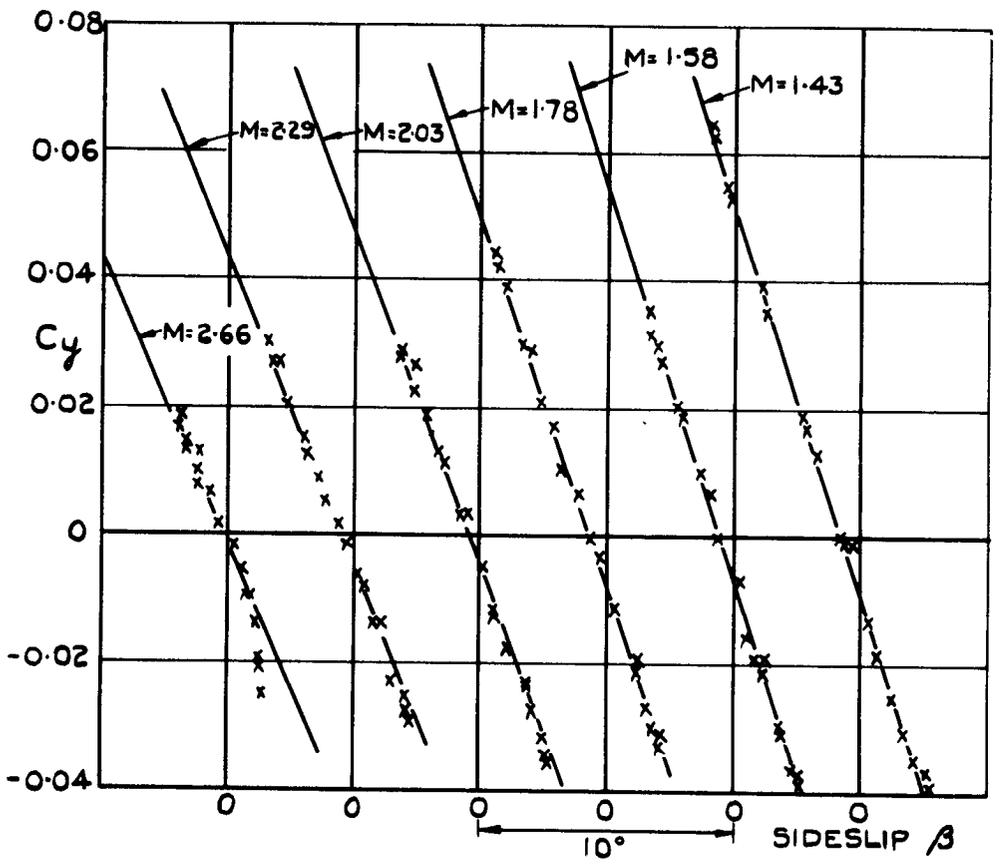

(b) SIDE-FORCE CURVES (MODEL 3)

FIG. 35. SIDE-FORCE CURVES (MODELS 2 & 3)

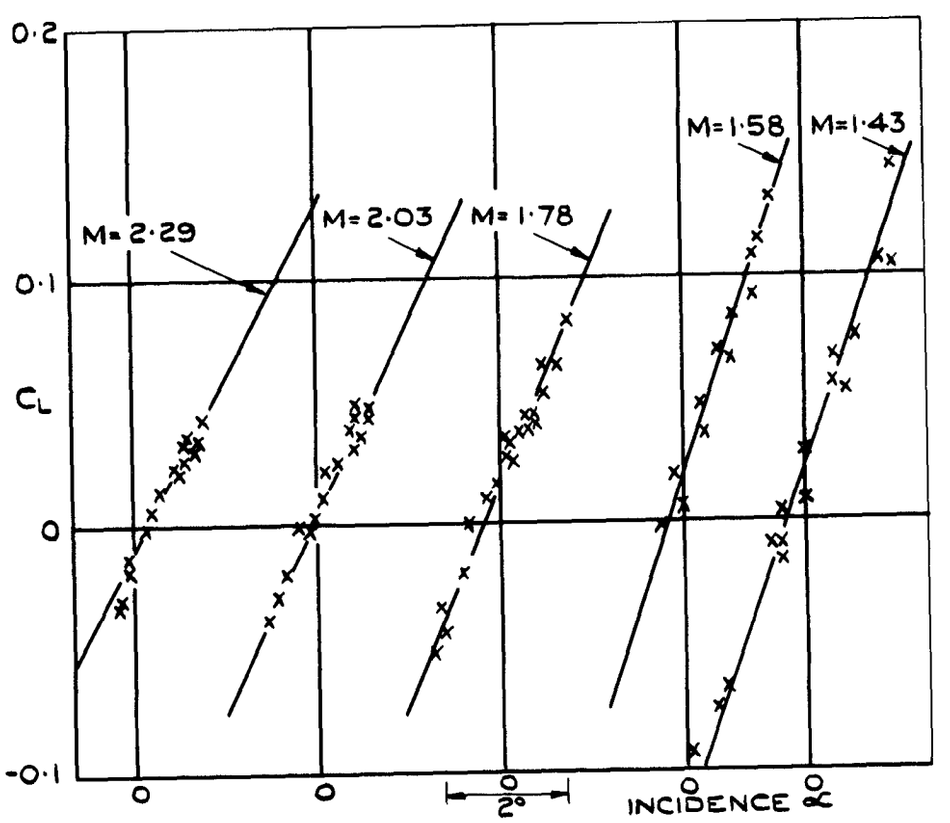

FIG. 36. LIFT CURVES (MODEL 3.)

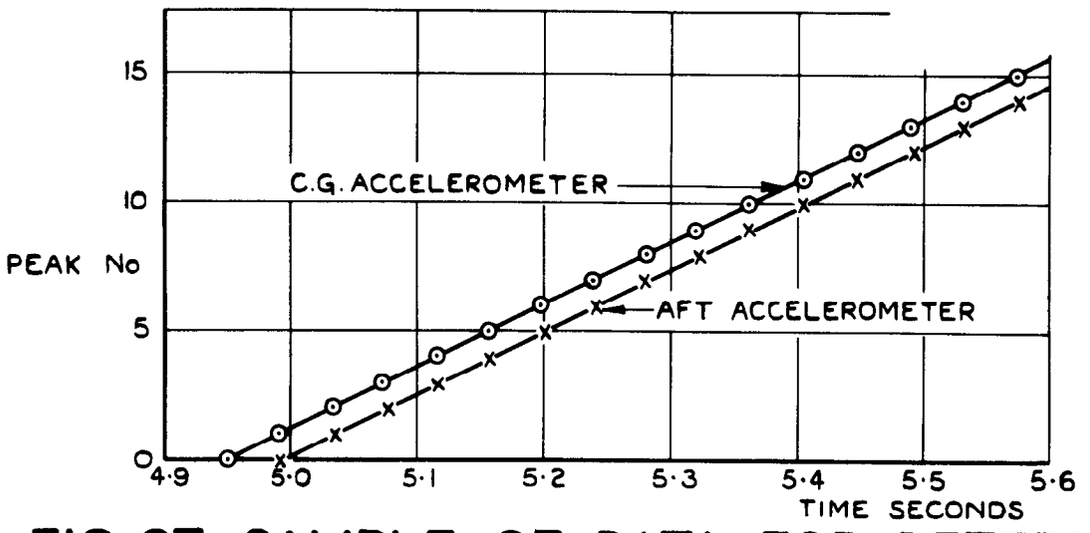

FIG. 37. SAMPLE OF DATA FOR DETERMINING FREQUENCY OF SHORT-PERIOD LONGITUDINAL OSCILLATION.
(MODEL 2, OSCILLATION 1)

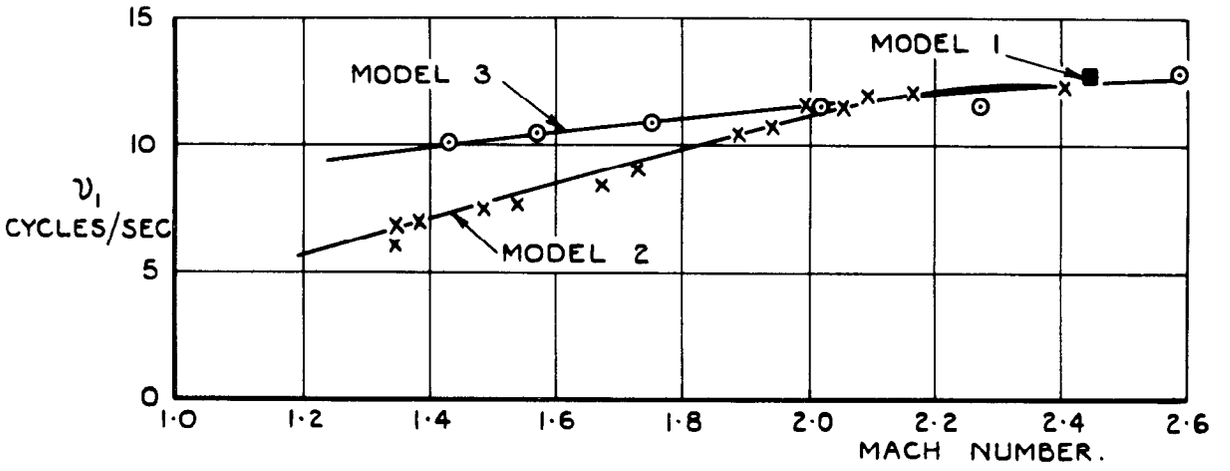

FIG. 38. NATURAL FREQUENCY OF SHORT-PERIOD LONGITUDINAL OSCILLATION.

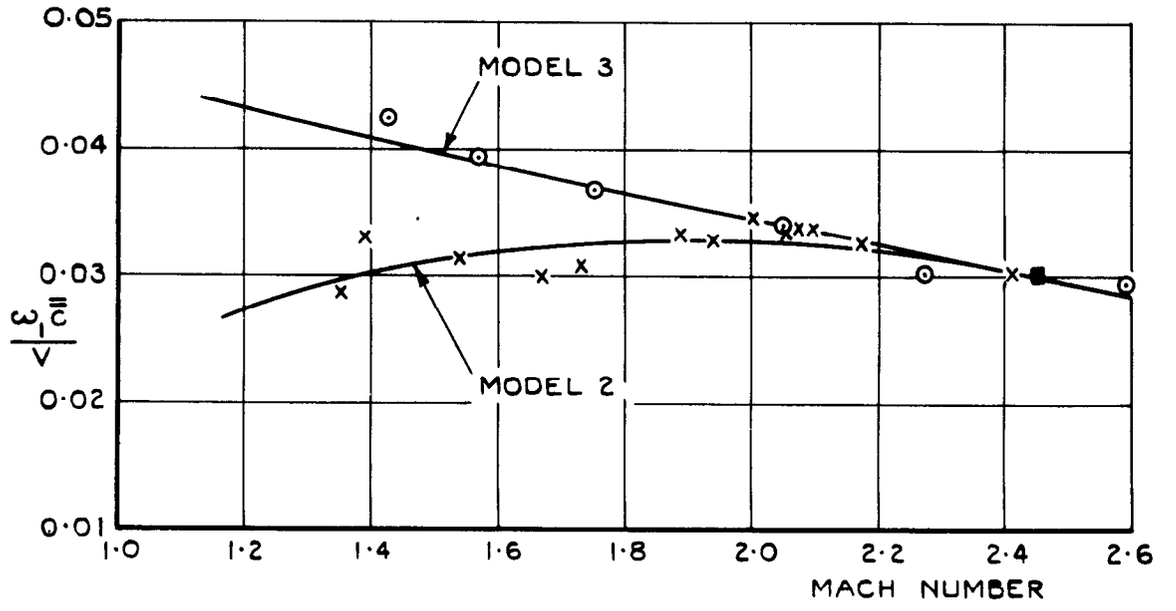

FIG. 39. NON-DIMENSIONAL FREQUENCY PARAMETER OF SHORT-PERIOD LONGITUDINAL OSCILLATION.

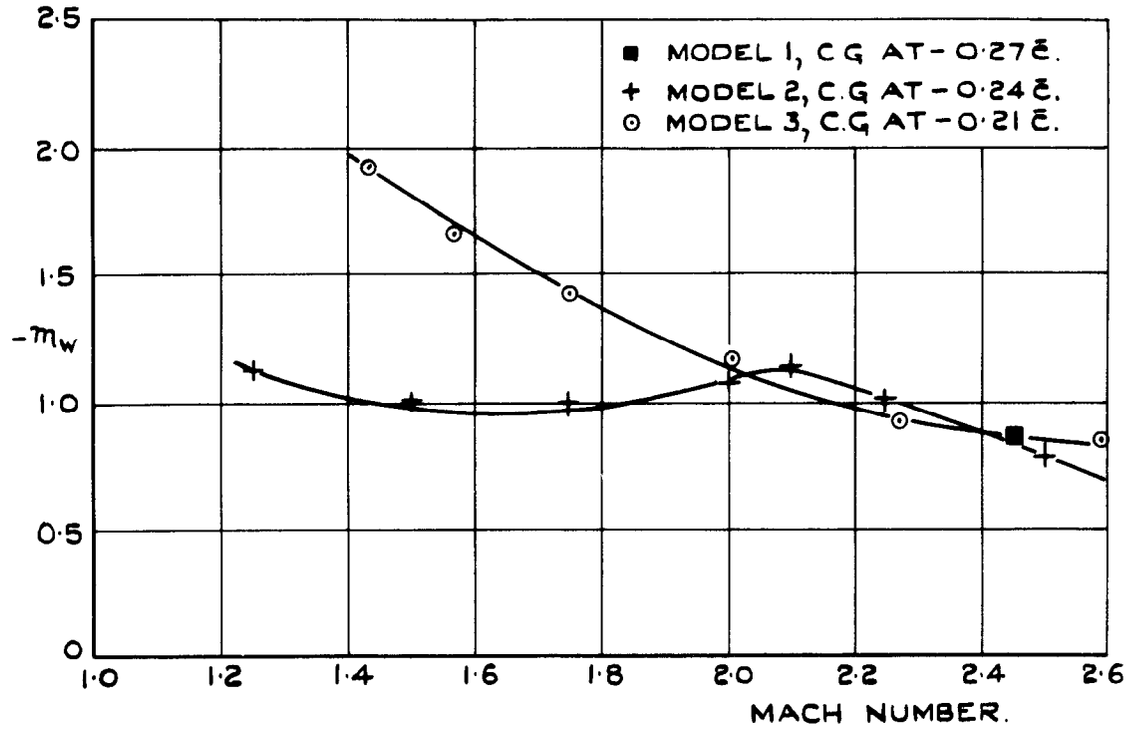

(a) MODELS 1,2 & 3.

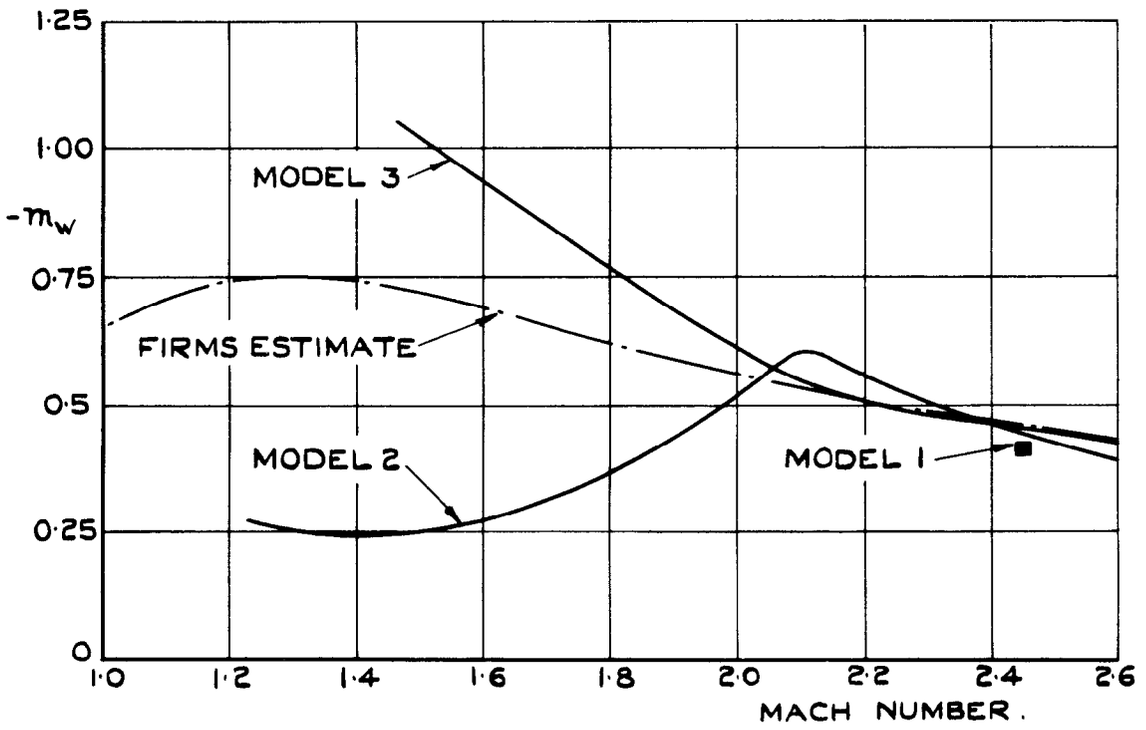

(b) MODELS 1,2 & 3 CORRECTED TO FULL-SCALE C.G. POSITION (+0·18c̄)

FIG.40. PITCHING-MOMENT DERIVATIVE m_w.

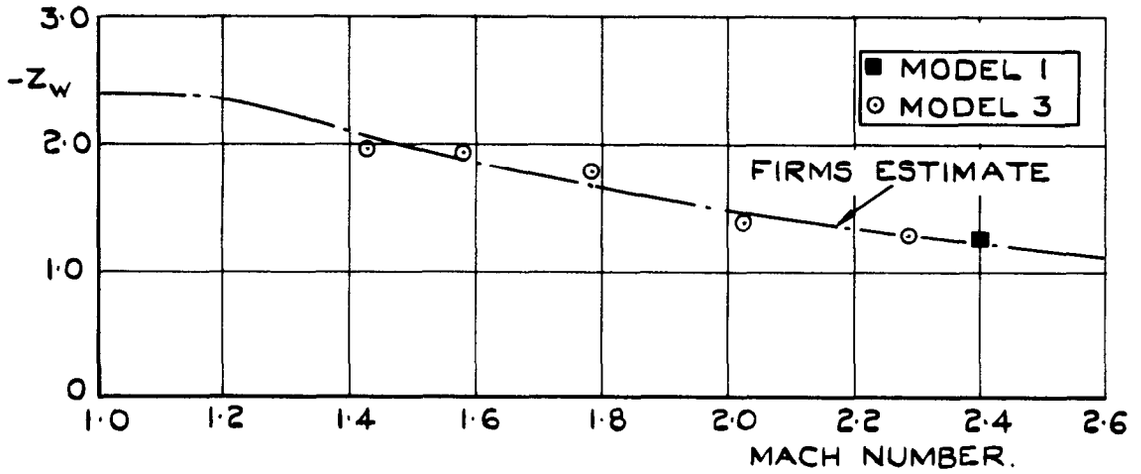

FIG.41. LIFT-FORCE DERIVATIVE z_w.

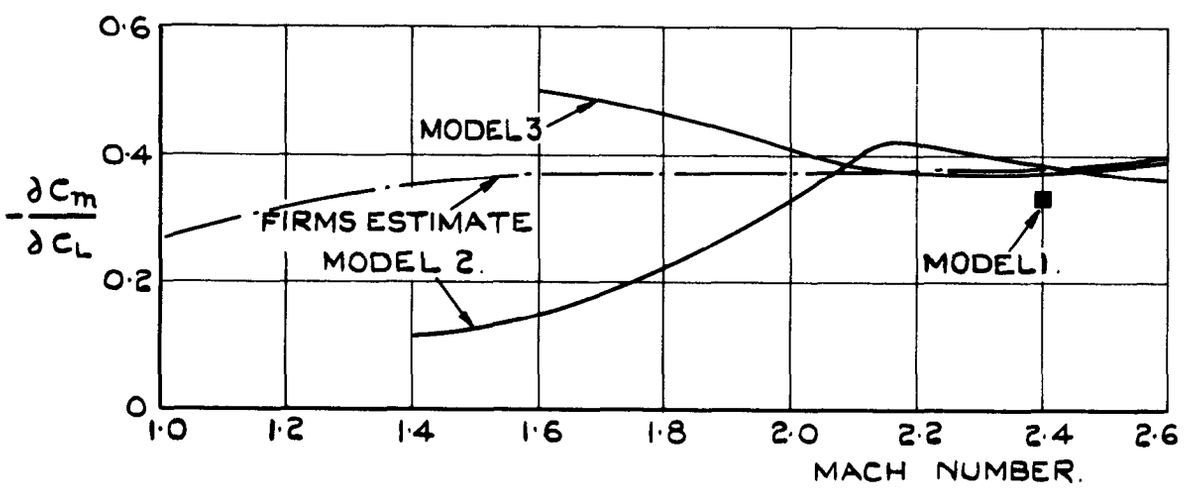

FIG.42. MANOEUVRE MARGIN (C.G AT -0·18$\bar{c}$)

Printed in England for Her Majesty's Stationery Office by the Royal Aircraft Establishment, Farnborough. W.T.60. K.4.

A.R.C. C.P. No.816

533.6.013.412 :
533.6.013.413 :
533.6.011.5 :
533.6.055 :
533.652.1

MEASUREMENTS OF DYNAMIC STABILITY FROM THREE SIMPLIFIED FREE-FLIGHT MODELS OF A SUPERSONIC RESEARCH AIRCRAFT (BRISTOL 188) OVER THE MACH NUMBER RANGE 1.2 - 2.6

Turner, K. J. March, 1961.

Values of the lateral stability derivatives y_v, n_v, ℓ_v and ℓ_p have been measured on free-flight models of the Bristol 188 for Mach numbers between 1.2 and 2.6. These show that the aircraft should be laterally stable up to M = 2.6, at least, although the free-flight results indicate a somewhat smaller stability margin than estimates or wind-tunnel measurements.

Some additional data on z_w and m_w have been derived from the longitudinal motion.

A.R.C. C.P. No.816

533.6.013.412 :
533.6.013.413 :
533.6.011.5 :
533.6.055 :
533.652.1

MEASUREMENTS OF DYNAMIC STABILITY FROM THREE SIMPLIFIED FREE-FLIGHT MODELS OF A SUPERSONIC RESEARCH AIRCRAFT (BRISTOL 188) OVER THE MACH NUMBER RANGE 1.2 - 2.6

Turner, K. J. March, 1961.

Values of the lateral stability derivatives y_v, n_v, ℓ_v and ℓ_p have been measured on free-flight models of the Bristol 188 for Mach numbers between 1.2 and 2.6. These show that the aircraft should be laterally stable up to M = 2.6, at least, although the free-flight results indicate a somewhat smaller stability margin than estimates or wind-tunnel measurements.

Some additional data on z_w and m_w have been derived from the longitudinal motion.

A.R.C. C.P. No.816

533.6.013.412 :
533.6.013.413 :
533.6.011.5 :
533.6.055 :
533.652.1

MEASUREMENTS OF DYNAMIC STABILITY FROM THREE SIMPLIFIED FREE-FLIGHT MODELS OF A SUPERSONIC RESEARCH AIRCRAFT (BRISTOL 188) OVER THE MACH NUMBER RANGE 1.2 - 2.6

Turner, K. J. March, 1961.

Values of the lateral stability derivatives y_v, n_v, ℓ_v and ℓ_p have been measured on free-flight models of the Bristol 188 for Mach numbers between 1.2 and 2.6. These show that the aircraft should be laterally stable up to M = 2.6, at least, although the free-flight results indicate a somewhat smaller stability margin than estimates or wind-tunnel measurements.

Some additional data on z_w and m_w have been derived from the longitudinal motion.

Published by
HER MAJESTY'S STATIONERY OFFICE

To be purchased from
York House, Kingsway, London w.c.2
423 Oxford Street, London w.1
13A Castle Street, Edinburgh 2
109 St. Mary Street, Cardiff
39 King Street, Manchester 2
50 Fairfax Street, Bristol 1
35 Smallbrook, Ringway, Birmingham 5
80 Chichester Street, Belfast 1
or through any bookseller

C.P. No. 816

S.O. CODE No. 23-9016-16